

## Semester Thesis

# Design and Testing of a Jumping Tensegrity Robot for Space Locomotion

Spring Term 2024



## **Declaration of Originality**

I hereby declare that the written work I have submitted entitled

**Design and Testing of a Jumping tensegrity Robot for Space Locomotion**

is original work which I alone have authored and which is written in my own words.<sup>1</sup>

### **Author(s)**

Jonathan Green

### **Student supervisor(s)**

Robert Baines  
Fabian Tischhauser

### **Committee members(s)**

### **Supervising lecturer**

Marco Hutter

With the signature I declare that I have been informed regarding normal academic citation rules and that I have read and understood the information on ‘Citation etiquette’ (<https://www.ethz.ch/content/dam/ethz/main/education/rechtliches-abschluesse/leistungskontrollen/plagiarism-citationetiquette.pdf>). The citation conventions usual to the discipline in question here have been respected.

The above written work may be tested electronically for plagiarism.

Zürich, 28/06/2024  
Place and date

  
Signature

<sup>1</sup>Co-authored work: The signatures of all authors are required. Each signature attests to the originality of the entire piece of written work in its final form.

# Intellectual Property Agreement

The student acted under the supervision of Prof. Hutter and contributed to research of his group. Research results of students outside the scope of an employment contract with ETH Zurich belong to the students themselves. The results of the student within the present thesis shall be exploited by ETH Zurich, possibly together with results of other contributors in the same field. To facilitate and to enable a common exploitation of all combined research results, the student hereby assigns his rights to the research results to ETH Zurich. In exchange, the student shall be treated like an employee of ETH Zurich with respect to any income generated due to the research results.

This agreement regulates the rights to the created research results.

## 1. Intellectual Property Rights

1. The student assigns his/her rights to the research results, including inventions and works protected by copyright, but not including his moral rights ("Urheberpersönlichkeitsrechte"), to ETH Zurich. Herewith, he cedes, in particular, all rights for commercial exploitations of research results to ETH Zurich. He is doing this voluntarily and with full awareness, in order to facilitate the commercial exploitation of the created Research Results. The student's moral rights ("Urheberpersönlichkeitsrechte") shall not be affected by this assignment.
2. In exchange, the student will be compensated by ETH Zurich in the case of income through the commercial exploitation of research results. Compensation will be made as if the student was an employee of ETH Zurich and according to the guidelines "Richtlinien für die wirtschaftliche Verwertung von Forschungsergebnissen der ETH Zürich".
3. The student agrees to keep all research results confidential. This obligation to confidentiality shall persist until he or she is informed by ETH Zurich that the intellectual property rights to the research results have been protected through patent applications or other adequate measures or that no protection is sought, but not longer than 12 months after the collaborator has signed this agreement.
4. If a patent application is filed for an invention based on the research results, the student will duly provide all necessary signatures. He/she also agrees to be available whenever his aid is necessary in the course of the patent application process, e.g. to respond to questions of patent examiners or the like.

## 2. Settlement of Disagreements

Should disagreements arise out between the parties, the parties will make an effort to settle them between them in good faith. In case of failure of these agreements, Swiss Law shall be applied and the Courts of Zurich shall have exclusive jurisdiction.

Zürich, 28/06/2024  
Place and date

  
Signature

# Contents

<b>Abstract</b>	<b>v</b>
<b>Symbols</b>	<b>vii</b>
<b>1 Introduction</b>	<b>1</b>
1.1 Overview . . . . .	1
1.2 Tensegrity Robots . . . . .	1
1.3 Existing Work . . . . .	3
1.4 Motivation . . . . .	3
1.5 Objectives . . . . .	4
<b>2 Hardware Development</b>	<b>7</b>
2.1 Feasibility . . . . .	7
2.2 Hardware Overview . . . . .	8
2.3 Structure . . . . .	8
2.3.1 Strut Assemblies . . . . .	8
2.3.2 Structural Topology . . . . .	9
2.3.3 Scaling Laws . . . . .	10
2.3.4 Tensegrity Structure Development . . . . .	10
2.4 Actuation . . . . .	15
2.4.1 Actuation Topology . . . . .	15
2.4.2 Actuator Development . . . . .	15
2.4.3 Actuator Performance . . . . .	19
<b>3 Testing and Evaluation</b>	<b>21</b>
3.1 Testing Methodology . . . . .	21
3.1.1 Data Collection . . . . .	21
3.1.2 Data Analysis . . . . .	21
3.2 Results . . . . .	22
3.2.1 Vertical Jumping . . . . .	22
3.2.2 Directional Jumping . . . . .	23
3.2.3 Self-Righting . . . . .	24
3.2.4 Tensegrity Properties . . . . .	24
3.2.5 Tumbling . . . . .	26
3.2.6 Stability Bifurcation . . . . .	26
3.3 Discussion . . . . .	26
3.3.1 Impact Resistance . . . . .	26
3.3.2 Friction . . . . .	26
3.3.3 Jumping . . . . .	27
3.3.4 Form and Volume Control . . . . .	28
3.3.5 Implementation Issues . . . . .	29
3.3.6 Measurement Error . . . . .	29

3.4	Evaluating Objectives . . . . .	30
3.5	Comparison to Existing Work . . . . .	31
<b>4</b>	<b>Conclusion</b>	<b>33</b>
4.1	Summary of Findings . . . . .	33
4.2	Limitations . . . . .	33
4.3	Further Research . . . . .	34
	<b>Bibliography</b>	<b>37</b>
	<b>A Additional Material</b>	<b>39</b>
A.1	Feasibility Modelling . . . . .	39
A.2	Scaling Laws . . . . .	40
A.3	Strut Failure . . . . .	40
A.3.1	Average Impact Force . . . . .	40
A.3.2	Failure Modes . . . . .	40
A.4	Spring Modelling . . . . .	41
<b>B Bills of Materials</b>		<b>43</b>
B.1	Actuator Bill of Materials . . . . .	43
B.2	Series Elastic Cable Bill of Materials . . . . .	43
B.3	Node Bill of Materials . . . . .	44
B.4	Robot Bill of Materials . . . . .	44
<b>C Datasheets</b>		<b>45</b>

# Abstract

Tensegrity robots are actuated structures comprised of a set of rigid members held in place by a network of tensioned cables. These robots have a series of physical properties that make them very well suited to space exploration, in particular exploration of foreign planets. Jumping as a form of locomotion for tensegrity robots offers additional benefits in these environments.

This work demonstrates the the feasibility of jumping as a form of locomotion for tensegrity robots. In particular, it focusses on jumping through actuation of the underlying tensegrity structure of the robot. First, a novel concept for a jumping tensegrity robot is investigated. This concept is then developed into a prototype robot, in parallel with the development of purpose-built actuators. Finally, the prototype jumping tensegrity robot is tested and evaluated to show feasibility of the approach of jumping by actuating the tensegrity structure and demonstrate the favourable properties of the robot.



# Symbols

## Symbols

$h_{max}$	Maximum jump height
$e_i$	Impact efficiency
$F_{max}$	Maximum actuator force
$k$	Stiffness of series-elastic structural cable
$m$	Mass of robot
$g$	Gravity
$F_{impact,avg}$	Average impact force
$t_{impact}$	Impact duration
$h$	Height of robot
$m_{spring}$	Mass of spring
$\alpha$	Constant representing material properties of spring
$d_{wire}$	Diameter of spring wire
$l_{spring}$	Length of spring
$E_{def}$	Energy required to deform structure
$F_{def}$	Force required to deform structure
$k_{struct}$	Elastic constant approximating stiffness of robot structure
$E_{KV}$	Translational kinetic energy in vertical direction
$E_{EP}$	Elastic potential energy
$F_{buckle}$	Critical buckling force
$E$	Young's modulus
$I$	Second moment of area of cross section
$r_{outer}$	Outer diameter of tube
$r_{inner}$	Inner diameter of tube
$D_{spring}$	Diameter of spring
$v_{torus}$	Volume of torus
$\rho_{wire}$	Density of spring wire
$G$	Modulus of rigidity
$F_{yield}$	Compressive failure load
$\rho_{yield}$	Compressive yield strength
$A_{strut}$	Cross-sectional area of strut
$\emptyset$	Diameter

## **Acronyms and Abbreviations**

BL	Body Length
CFRP	Carbon-Fibre Reinforced Polymer
CoM	Centre of Mass
CotS	Commercial off the Shelf
FFF	Fused Filament Fabrication
MJF	Mulit Jet Fusion
PLA	Polylactic Acid
TPU	Thermoplastic Polyurethane
UHMWPE	Ultra-High Molecular Weight Polyethylene

# Chapter 1

## Introduction

### 1.1 Overview

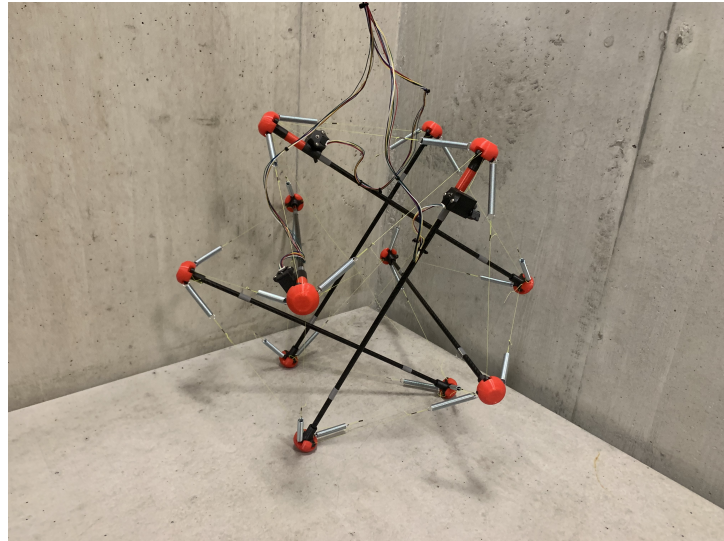


Figure 1.1: The prototype jumping tensegrity robot

This work presents a novel tensegrity robot capable of jumping locomotion through actuation of the underlying tensegrity structure (figure 1.1). Chapter 1 provides background on tensegrity robotics, discusses relevant existing work in the field of jumping tensegrities, and formulates a set of objectives. Chapter 2 then discusses the development of the robot itself, outlining key aspects of its design and justifying significant design decisions. Chapter 3 provides detail about the testing of the robot, showcases and discusses the results, and evaluates these results in the context of the objectives and in comparison to other tensegrity robots. Finally, chapter 4 summarises the findings, considers the limitations of this work, and proposes further avenues of research.

### 1.2 Tensegrity Robots

Tensegrities are structures created by a system of discontinuous rigid struts held in an equilibrium configuration by a network of tensioned cables [1]. A key

aspect of tensegrities is that they do not have any direct contact between struts, yielding a structure with low overall stiffness [2]. The presence of stiff components in conjunction with a high overall softness allows tensegrity robots to draw beneficial properties from both soft robotics and from more conventional stiff robotics [3].

An inherent property of tensegrities is that the rigid members experience only axial compression, while the cables experience only axial tension. The subsequent lack of bending moments and radial forces allow the mass of the structures to be minimised while maintaining a high resistance to impact damage [3]. Similarly, the lack of stiff interfaces between the rigid components of the structures and the network-style interconnection of cables distributes external forces throughout the structure and prevents high force concentrations that could cause damage [4].

With the inclusion of elastic elements (specifically cables that act as tensile springs, struts that act as compressive springs, or a combination of both) the structure can be designed to have a high overall compliance. This further increases the resistance to damage, and allows energy to be stored in the deformation of the structure. This high compliance also allows tensegrity structures to experience very significant changes in form without damage [5].

When augmented with actuators to become tensegrity robots, tensegrities can be used to carry out a broad range of tasks. Specifically, by changing the length of the struts or the length of the cables, the equilibrium form of the structure will change. This change in form can be exploited for tasks such as manipulation [6] or locomotion [3]. In these robots, the presence of rigid components allows the use of more conventional actuators and off-the-shelf robotics components while the structure can still have many of the useful properties of a soft robot given its overall compliance.

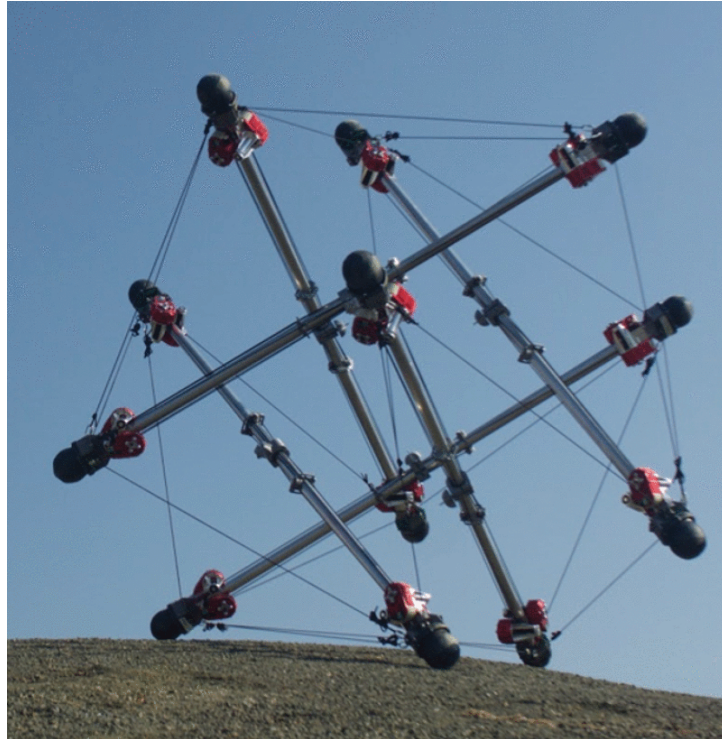


Figure 1.2: NASA's SUPERball v2 [7]

### 1.3 Existing Work

A broad range of tensegrity robots have been developed. Many, such as NASA's SUPERball v2 (figure 1.2) are capable of locomotion by punctuated rolling - a process in which the robot repeatedly shifts its centre of mass (CoM) to tip onto a desired face [7]. This style of locomotion has been widely used. However, it is typically slow (on the order of a few body lengths (BL) per minute [3]) and inefficient (the robot must deform by a large amount for each small translation).

Significant work has gone into the development of better gaits for tensegrity robots, including through the use of genetic algorithms [8] and deep reinforcement learning [9]. While these approaches yielded more sophisticated gaits, they are still relatively slow with a maximum locomotion speed of 0.025BL/s [8] and 0.07BL/s [9] respectively.

To account for the issues associated with tensegrity locomotion on the ground, alternative methods such as hopping and jumping have been proposed. These are enabled with the use of additional actuators, including thrusters [10], propellers [11][12] (figure 1.3), and highly dynamic actuators that impact against the ground to produce thrust [13]. These improve efficiency and speed, and allow the robot to avoid obstacles by jumping over them.

However, these methods do not exploit the useful properties of the tensegrity structure when jumping. Specifically, due to their high compliance, tensegrity structures can store and release a large amount of elastic potential energy through deformation of their structure. This is amplified by their ability to sustain very significant deformations without damage. Limited work has been done to exploit this as a mechanism for jumping, in which the underlying tensegrity structure itself is actuated. In [14], small jumps are demonstrated by actuating the tensegrity structure with shape-memory alloy springs, but these jumps did not exceed a height of 0.98BL. A high jumping (defined here as >1BL) tensegrity robot based on this concept has been proposed for planetary surface exploration in [15], however directional jumping was only possible by creating a lattice of several individual robots and high jumping was demonstrated only in simulation.

### 1.4 Motivation

The combination of high impact damage resistance, low mass, and large variability in form make tensegrities well suited to applications in space robotics. The resistance to impact damage makes tensegrities robust to the harsh conditions of operation on foreign planets; in fact it has been proposed that if a tensegrity can survive impacts at its terminal velocity then it may be deployed on a foreign planet by simply being dropped from orbit, removing the need for a dedicated lander and complex landing procedure [16]. Additionally, being able to change the shape of the robot significantly means that tensegrity robots can pack into small volumes or unusually shaped spaces, to best make use of the limited room on a spacecraft. Their low mass is similarly beneficial for conserving spacecraft fuel.

The work presented in section 1.3 shows that jumping is a promising form of locomotion for tensegrities. These benefits are enhanced in low gravity environments; locomotion methods such as shuffling [8] and punctuated rolling [7] do not gain speed or efficiency when gravity is lower (since they must translate their CoM horizontally by the same amount per step regardless of gravity), while a jumping robot can travel further with the same amount of energy than in higher gravities. However, very limited research has been done into jumping utilising the underlying tensegrity structure of the robot. Actuating the underlying structure has potential to enable higher and further jumps, reduce overall complexity of the robot, and im-



Figure 1.3: A tensegrity robot that can jump using propellers [12]

prove efficiency of locomotion. In addition, while thrusters and propellers need to be tailored to specific atmospheric conditions for optimum performance, jumping with the tensegrity structure itself has no atmospheric requirements.

Hence, the fundamental research question addressed in this work is: can the feasibility of jumping as a form of locomotion for tensegrity robots be demonstrated on hardware through actuation of the underlying tensegrity structure?

## 1.5 Objectives

To address the question described in section 1.4, the following objectives have been formulated:

1. The robot should be able to jump high. High is defined as  $>1.0BL$
2. The robot should be able to jump in a controlled direction. When a direction is selected, the robot should reliably jump  $>0.5BL$  in that direction
3. The robot should be configuration agnostic, meaning it can jump no matter how it is oriented. Specifically, it should be able to achieve objectives 1. and 2. regardless of which face it is resting on.. This is important for locomotion as the robot may tumble upon landing from a jump, and must be able to jump again regardless of the orientation in which it comes to rest to locomote reliably
4. The robot should fulfil objectives 1., 2., and 3. by changing the shape of the tensegrity structure rather than with separate actuators such as thrusters or propellers.

5. The robot should demonstrate the favourable properties of tensegrity structures. Specifically, it should:
  - (a) Be capable of surviving large impacts (drops from  $>5.0\text{BL}$  height and impact velocities of  $>10.0\text{BL/s}$ ) without sustaining permanent damage)
  - (b) Have a high strength to mass ratio (accomplish objective 5a. with a mass of  $<1\text{kg}$ )
  - (c) Be capable of significant changes in form without sustaining permanent damage (reduction in volume of  $>2x$ )



# Chapter 2

# Hardware Development

## 2.1 Feasibility

To ensure that it was feasible to construct a robot that was capable of jumping more than one body length, a simplified model of the system was developed and evaluated (see appendix A.1). This yielded the following approximation of maximum jump height  $h_{max}$ :

$$h_{max} = \frac{3e_i F_{max}^2}{kmg} \quad (2.1)$$

Where impact efficiency  $e_i$  describes the proportion of elastic potential energy stored in structural deformation that is converted to vertical translational energy,  $F_{max}$  is the maximum actuator tensioning force,  $k$  is the stiffness of the elastic structural cables,  $m$  is the mass of the robot, and  $g$  is gravity.

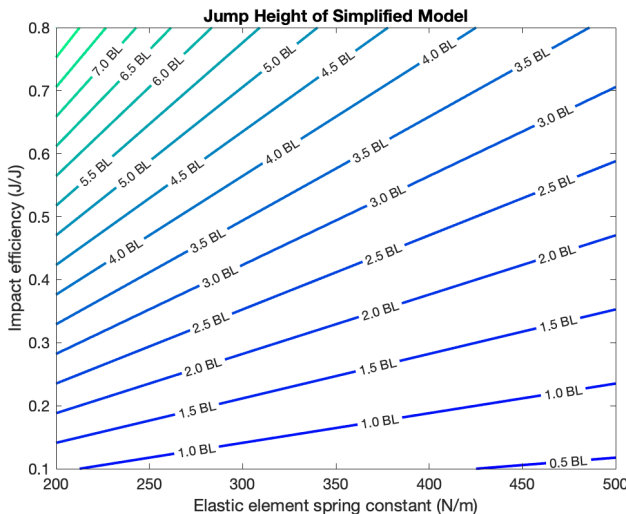


Figure 2.1: Predicted robot jump height in terms of body lengths. “Impact Efficiency” describes the proportion of stored energy converted into vertical motion during the jump (appendix A.1). Body length was defined as 0.6m, as the exact size of the robot was not known at the time of simulation

The results, seen in figure 2.1, show that even if as little as 15% of energy stored in the structure is converted to vertical motion, it is still possible to achieve jumps

in excess of one body length in height if the robot is designed suitably. Specifically, the robot should have a stiffness of  $<450\text{N/m}$  for the elastic cables, a maximum actuator force of  $>50\text{N}$ , and a mass of  $<600\text{g}$  (see appendix A.1). This was a necessary first step in hardware development to ensure that it would be possible to achieve the objectives described in section 1.5.

## 2.2 Hardware Overview

Table 2.1: Composition of the robot

Item	Mass (g)	Quantity	Material
Spring	7.9	24	Zinc-Plated Steel
Structural Cable	$<0.1$	24	Braided UHMWPE
Actuator Cable	$<0.1$	3	Braided UHMWPE
Node*	5.6	12	PLA, with metal fasteners
Node Compliant Endcap	6.1	12	TPU
Strut	10.5	6	CFRP
Actuator*	35.7	3	Mixed
Decoupling Bumper	2.4	3	TPU
Total	507.3		

\* Including all sub-components (such as fasteners, bearings, gears, and motors).  
See appendix B.3 and appendix B.1 for details

A prototype robot was developed with computer-aided design (CAD) (figure 2.3), prototyped, and built (figure 1.1). The hardware of the robot was designed to best address and fulfil the objectives outlined in section 1.5. This required the development of both the underlying tensegrity structure and of a method of actuation capable of manipulating the structure to induce satisfactory jumps. The completed robot has a diameter of 610mm. The robot's form is best described by a Jessen's icosahedron (which has several possible size metrics), so diameter here refers to the smallest sphere that fully contains the robot. It has a mass of 507g (see table 2.2), excluding the tether used to power the robot. The tensegrity structure is comprised of six strut assemblies and 24 series-elastic cables. This structure is augmented with three actuators that control the tension on three inelastic actuator cables. The series-elastic structural cables are pre-tensioned to 12.5N.

The robot is modular to assist with ease of assembly and to reduce the number of unique parts that need to be designed and fabricated. This means that the robot can be divided into groups of components (strut assemblies, actuators, series elastic structural cables) in which every element is identical.

## 2.3 Structure

The structure of the robot is the underlying tensegrity object that gives the robot its form. Tensegrity is a broad class that covers a very wide range of assemblies, many of which have varied properties dependent on their particular geometry. It was therefore important to design and construct a tensegrity structure that had suitable properties for jumping to be the basis of the robot.

### 2.3.1 Strut Assemblies

The robot was designed as six strut assemblies (figure 2.2) connected by a set of tensioned series-elastic cables. Each strut assembly is comprised of a carbon-fibre

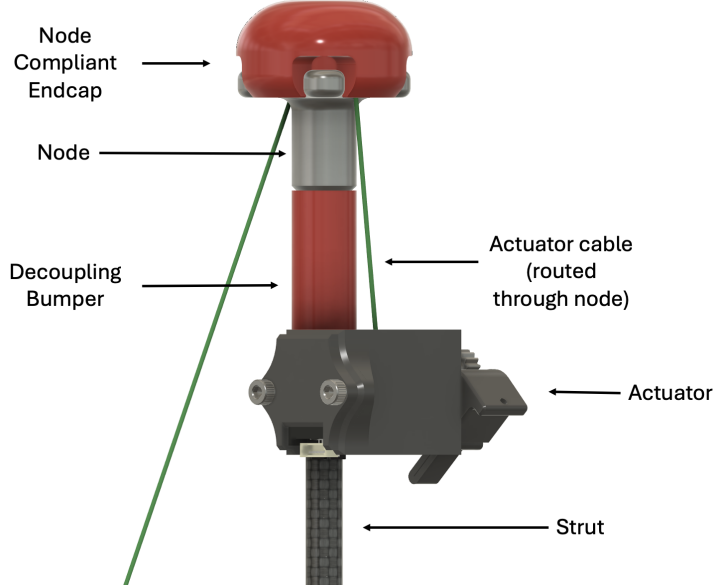


Figure 2.2: One end of a strut assembly. The other end of the strut is similar, although as it is unactuated it lacks the actuator, decoupling bumper, and actuator cable. Three of the six strut assemblies have an actuator at one end, and three are unactuated.

reinforced polymer (CFRP) tube (see section 2.3.4) that forms the body of the strut, and a node assembly at either end. The nodes act as the attachment points for the cables and springs, and have a slot for the actuator cable to run through them (see section 2.3.4 for details). Additionally, three of the six strut assemblies have actuators mounted below the node. To protect the actuators from the large forces that they may experience during impacts, they are decoupled from the structure and mounted within its bounding polyhedron (see section 2.4.2).

### 2.3.2 Structural Topology

In the taxonomy of tensegrity structures described in [2], a  $k$ -class tensegrity contains  $k$  rigid bodies in direct contact. This work considers only 0-class tensegrities, as these provide the best opportunity to satisfy objectives 5a. and 5c. (section 1.5).

To select a suitable topology, the following requirements were defined for candidate tensegrity structures:

1. The structure should be capable of significant deformation, so that it may absorb a large amount of energy. This is beneficial for resistance to impact damage, and allows energy to be stored in the structure to be used for jumping.
2. The structure should have symmetry such that, when resting on a face described by a particular polygon, it is in a configuration indistinguishable from configurations resting on any other face described by the same polygon. This is commonly described as a spherical tensegrity [5] as their outer surface approximates a sphere. The purpose of enforcing this form of symmetry is to facilitate configuration-agonistic jumping by making the robot's rest configuration independent of the face that it is resting on.
3. The structure should have support polygons such that, when resting on the ground, none of the struts are orthogonal to the ground. This is to ensure

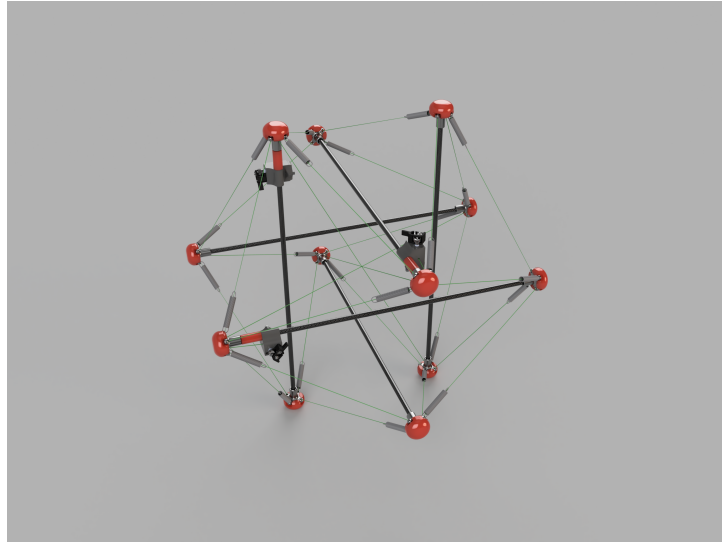


Figure 2.3: A render of the prototype robot in CAD

robustness of the structure, as the structure is least elastic when an external force applied is orthogonal to the struts.

The six-bar icosahedron tensegrity was chosen to meet these requirements. Experimentation with scale models, and work in simulation [17] suggested that this topology was the minimal structure capable of satisfying the requirements. Selecting the minimal structure helped reduce complexity and mass. Additionally, this structure is very widely used for similar tensegrity robots [7] [10] [12] [13] [14] [18].

### 2.3.3 Scaling Laws

The physical size of the prototype was an important aspect to consider. Existing tensegrity robots vary greatly in size, from the centimetre scale [12] to the multi-metre scale [7]. Given that higher and further jumps can be achieved by minimising mass and maximising jump energy, the scaling laws associated with the energy to mass ratio of the robot were explored. Specifically, under the simplifying assumptions described in section 2.1 the ratio of stored elastic potential energy  $E_{EP}$  to mass  $m$  follows

$$\frac{E_{EP}}{m} \propto \frac{F_{max}^2}{kl} \quad (2.2)$$

Where the structure has strut length  $l$  (see appendix A.2)

Since the ratio in equation 2.2 grows faster with actuator force than with inverse strut length, focus was placed developing a more capable actuator rather than on optimising strut length. Hence, the strut length was chosen to be 500mm, as this provided ample space for the inclusion of actuator and made the structure easy to handle. The decision to fix this parameter early allowed other structural parameters to be tuned.

### 2.3.4 Tensegrity Structure Development

Designing the structure itself was a process that required balancing the competing requirements of high strength and low mass. All parts outlined in this section were tested extensively with static loads to determine their failure point before the

prototype robot was assembled. This testing was to ensure that deforming the structure during operation of the robot would not pose a safety risk.

### Struts

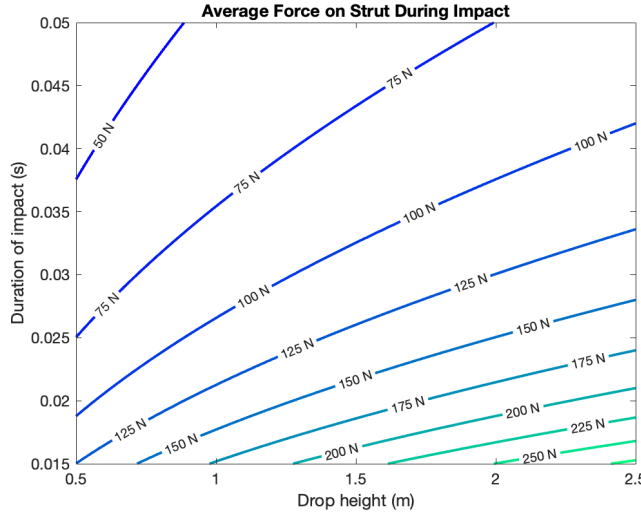


Figure 2.4: Worst case average force experienced by a strut during an impact

CFRP was chosen as the material for the struts due to its superior stiffness to weight and strength to weight ratios [19]. To further minimise weight and improve stiffness, hollow cylindrical sections were used.

The average force  $F_{impact,avg}$  experienced by a strut during an impact of duration  $t_{impact}$  when dropped from height  $h$  follows

$$F_{impact,avg} = \frac{m(2gh)^{\frac{1}{2}}}{t_{impact}} \quad (2.3)$$

This is considering the worst case impact, in which a single strut absorbs the full force of the impact, see appendix A.3 for the derivation. Plotting equation 2.3 shows that when dropped from heights of 2.5m then the strut may be subjected to forces up to 325N if the impact occurs over a duration as short as 15ms (figure 2.4).

Failure of a strut would be extremely serious and could pose a risk to safety during testing due to the large amount of energy stored in the structure. Additionally, the peak force experienced during impact may be higher than average force. For these reasons, a safety factor of 2 was used, yielding a design requirement that the strut should sustain up to 650N before failure.

Analysing the failure modes of the struts (appendix A.3) shows that given the slenderness of the carbon fibre tubes, they will fail by buckling well before the material compressive strength limit is reached (figure 2.5).

Using this analysis, tubes of 8mm outer diameter with 0.5mm wall thickness were chosen, as these were the lowest mass option with an adequate critical buckling load (663N) that were readily available from suppliers.

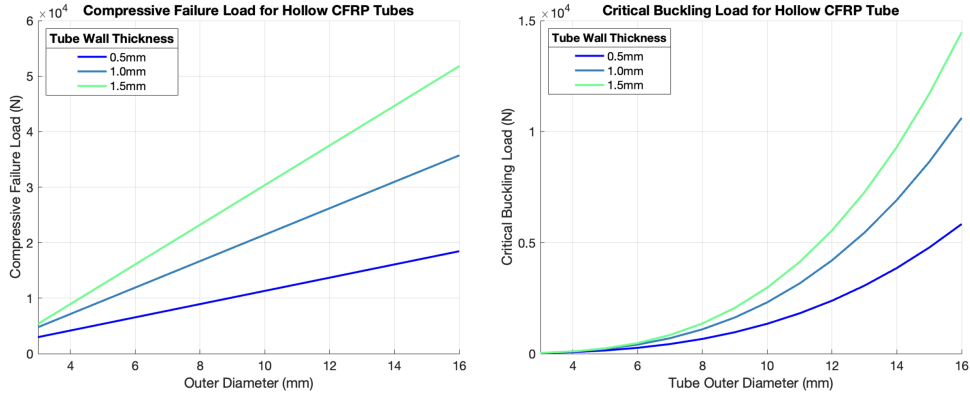


Figure 2.5: Failure of carbon fibre tubes due to compressive yielding (left) and buckling (right)

## Nodes

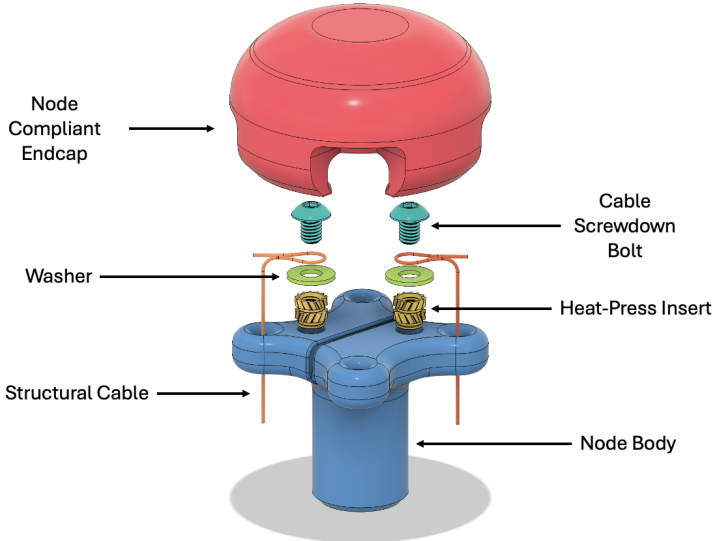


Figure 2.6: Exploded view of the node assembly. False colour used to improve interpretability

At the end of each strut is a node assembly (figure 2.6). These purposes of these nodes are:

- To provide an interface that allows cables and springs to be mounted to the end of the strut
- To protect the end of the strut during impacts
- To route the actuator cables over the end of the strut (see section 2.4.2)
- To allow for adjustment of the length of structural cables so that pretension can be adjusted
- To provide a point on the robot that can be tracked during testing. For motion capture, the node compliant endcap was covered in retro-reflective tape to enhance this ability

All nodes are identical to preserve modularity (despite only three having actuator cables running through them). Each node has four attachment points; two for cables and two for springs. Since each series-elastic structural cable is a spring at one end and a cable at the other, the node's four attachment points alternate which end of the series-elastic structural cable they attach to to maintain symmetry (and consequently symmetric mass distribution) on the structure. Each node has a compliant endcap, which is fused filament fabricated (FFF) 3D printed out of thermoplastic polyurethane (TPU). This endcap protects the cable and spring attachment points, provides additional energy absorbance during impacts, and increases ground friction to improve jump performance. The body of the node is FFF 3D printed out of polylactic acid (PLA) for ease of fabrication, and has a rounded slot for the actuator cable to pass through.

Springs are attached by looping their ends through the node body's mount holes. Cables are attached with a "screwdown" method, where a loop of cable is compressed between a washer and bolt-head (figure 2.6). Brass heat-press inserts provide screw holes that allow the screwdown cable clamps to be tightened without damaging the relatively soft plastic of the node body.

### Elastic Elements

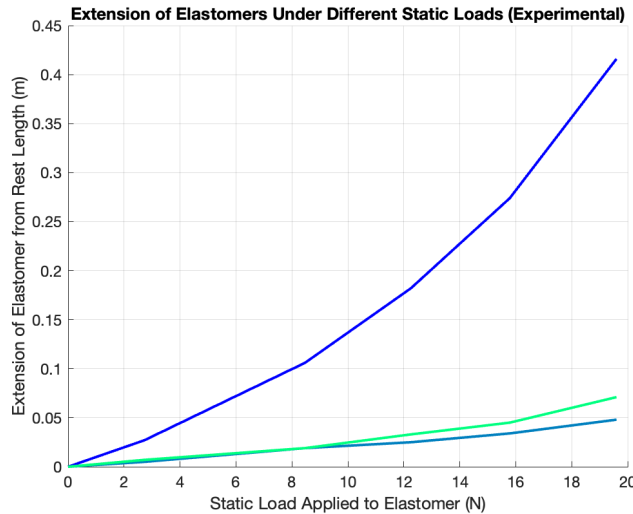


Figure 2.7: The force vs extension curves of three of the elastomers tested. All three display non-Hookean behaviour

Both elastomers and conventional extension springs were considered for use as elastic elements in the structural elastic cables.

Elastomers of a range of forms and stiffnesses were purchased and tested. Static load testing showed that they had significantly non-Hookean behaviour in the range of loads expected during use (figure 2.7). Additionally, when loads were sustained for more than a few seconds, relaxation of the elastomers was observed where the force they were exerting would slowly decrease. These non-linearities made modelling and simulation challenging, and for this reason conventional metallic springs were chosen instead.

Simulation showed that a spring stiffness of 400N/m would yield the highest jumps [17]. From equation 2.4 it can be seen that, in order to minimise mass for this spring stiffness, a spring should be selected that has the shortest length and

the narrowest wire diameter. This was used to select the optimal springs from the supplier's catalogue.

### Series Elastic Structural Cables

The structural cables must be elastic to allow for energy storage in deformation of the tensegrity, however they do not necessarily need to be elastic along their entire length. Given that mass was a primary concern when designing these elastic cables (the large number of them in the structure means that a small individual increase in mass will significantly increase the structure's mass), a series elastic approach was considered.

A spring model was developed (section A.4), which yielded the following formula for spring mass  $m_{spring}$ :

$$m_{spring} = \alpha d_{wire}^{\frac{8}{3}} l_{spring}^{\frac{2}{3}} \quad (2.4)$$

Where  $l_{spring}$  is the rest length of the spring,  $d_{wire}$  is the wire diameter, and  $\alpha$  is a constant representing the material properties of the spring and the desired spring stiffness (see section A.4).

From this it can be seen that shorter springs are desirable for lower mass, even though they may have larger coil diameter for a given stiffness. Given that the mass of the inelastic cable discussed in 2.3.4 is negligible, it is beneficial to construct the structural cables as series elastic cables, where each structural cable is composed of a long inelastic section and a short elastic spring.

### Inelastic Cables

The inelastic cables used for actuation and for the inelastic component of the series elastic structural cables were chosen to be ultra high molecular weight polyethylene (UHMWPE), due to its extremely high tensile strength, low friction, and high flexibility. Additionally, it is widely used for similar purposes in jumping robots in the literature [20] [21] [22].

However, due to the small diameter and low coefficient of friction, cable termination was difficult. A series of different termination methods were tested to determine their load capacity. The only methods capable of sustaining adequate loads were crimping with copper collars, and screwdown clamping (see 2.3.4).

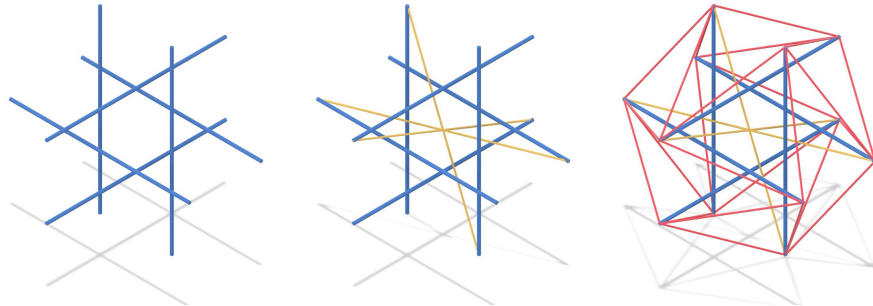


Figure 2.8: The tensegrity structure without any cables (left), with only the inelastic actuator cables (middle), and with both the inelastic actuator cables and the elastic structural cables (right)

## 2.4 Actuation

### 2.4.1 Actuation Topology

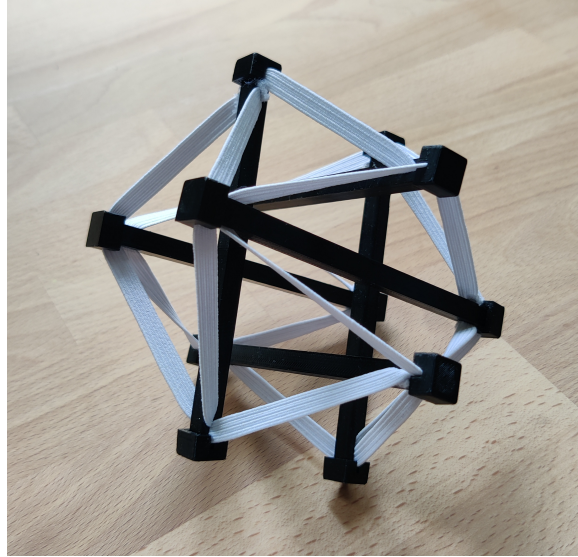


Figure 2.9: A scale model of the six-bar icosahedron tensegrity used for topology development

The actuation topology is the arrangement of actuators, cables, and struts within the tensegrity structure that allow the form of the structure to be controlled.

To develop an actuation topology, scale models of the six-bar icosahedron tensegrity were constructed (figure 2.9). Candidate actuation topologies were then generated from this scale model, and the candidates evaluated in simulation to determine the most appropriate one [17].

The “skew-central” actuation topology was determined to be the most suitable. In this topology, the underlying six-bar icosahedron tensegrity structure is augmented with three additional inelastic cables. These cables run between the diagonally opposite points in each pair of parallel struts (figure 2.8).

This topology was selected because it allowed for directional jumping with the minimum number of actuators (three) while also enabling larger deformation of the tensegrity structure than other topologies. These two aspects were well suited to the objectives of directional jumping and high jumping.

### 2.4.2 Actuator Development

The actuation topology described in 2.4.1 requires an actuator capable of changing the length of an inelastic cable under tension. Approximately modelling the tensegrity structure as a single spring with stiffness  $k_{struct}$ , the energy stored in deformation  $E_{def}$  when subject to deformation force  $F_{def}$  follows (appendix A.1)

$$E_{def} = \frac{F_{def}^2}{2k_{struct}}$$

Since the stored energy used for jumping grows quadratically, in order to jump high it is desirable for the actuator to have the highest maximum actuation force possible. The following requirements for an actuator were established. The actuator should:

1. Have a high maximum force capacity ( $>50\text{N}$ )
2. Have a low mass ( $<55\text{g}$ )
3. Be capable of changing the length of a cable under tension by a controlled amount (precision of  $\pm 5\text{mm}$  or better)
4. Be capable of maintaining a cable at constant length under high tension ( $<50\text{N}$ ) for a non-negligible amount of time
5. Be capable of releasing the tension in the cable during a short period ( $<100\text{ms}$ ) to enable the rapid release of energy required for jumping

Note that the numerical values for these requirements were drawn from the feasibility study outlined in 2.1, and from simulation in [17].

A range of actuation strategies drawn from the literature were considered. The final actuator design is a combined winch and clutch mechanism, drawing on an active clutch developed specifically for jumping robots in [20].

### Winch-clutch Mechanism

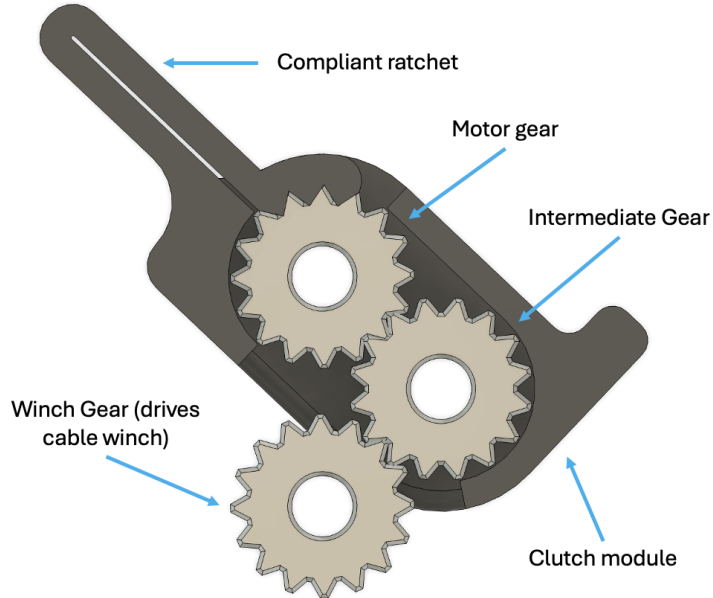


Figure 2.10: The clutch mechanism in the engaged position. Note that the top cover of the clutch module has been removed in this render so that the gears are visible

The actuator is built around a winch-clutch mechanism drawn from the active clutch developed for the JumpRoACH jumping robot [20]. The benefit of this mechanism is that it allows the winch winding, the clutch engagement, and the clutch disengagement to all be carried out by a single motor.

This mechanism is comprised of three gears and a clutch module with an integrated ratchet (figure 2.10). The motor drive gear and an intermediate gear are mounted within the clutch module, and the entire clutch module can pivot about the motor shaft. The third gear is attached to a pulley around which the inelastic actuator is wound.

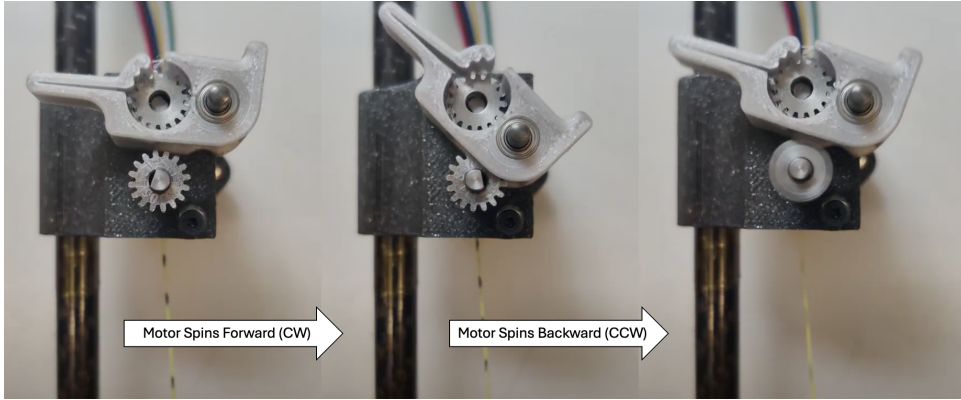


Figure 2.11: The process of engaging and disengaging the clutch. Initially, the clutch is disengaged (left). The motor is rotated forward and friction in the ratchet causes the clutch module to rotate with the motor drive gear, engaging the clutch (middle). The motor is then rotated backwards to lock the ratchet, which pivots the clutch module away from the winch gear, disengaging the clutch and allows the winch to turn freely and unwind (right)

The outcome is that when the motor rotates in the forward direction, the clutch is engaged and the winch will wind at a constant rate. The duration for which the motor is powered is then proportional to the change in length of the cable. A quadrature encoder is attached to the motor shaft to more accurately measure the change in cable length. The motor can then be rotated in the backward direction, which will disengage the clutch, allowing the winch to freely unwind and hence releasing the tension on the actuator cable. This process can be seen in figure 2.11.

Additionally, due to the high reduction ratio (986:1) gearbox on the output of the motor (figure 2.12), the mechanism is not back-driveable. This allows the actuator to maintain the high loads experienced during compression so that the robot can be held in any compressed state without power indefinitely.

### Actuator Decoupling

The actuators, containing several small moving components, are more fragile than the rest of the robot. Many tensegrity robots place actuators on the end of their struts [7] [23]. However, this poses an issue in jumping tensegrities where the ends of struts encounter large forces associated with impacts. To ensure that the actuators are protected during impacts, this robot instead places them within the bounding polyhedron of the tensegrity structure, ensuring the actuators will not contact the ground during impacts, even when the structure is deformed. To further protect the actuators, they are decoupled from the structure along the axis of actuator cable tension. In practice the means that the actuators are mounted to the struts of the robot with collars that can slide up and down the strut (figure 2.2). The actuator cables have a small amount of slack. When the actuator begins winding in the cable, the actuator takes up the slack in the cable and is pulled up the strut to contacts a compliant bumper. This locks it in place and couples it to the structure, allowing it to tensions the actuator cables and compress the structure. When tension is released for a jump the actuator is once again decoupled, ensuring that if there is a spontaneous high force on the actuator cable (such as the “jerk” experienced during impact induced deformation) the actuator can move and does not need to absorb the force.

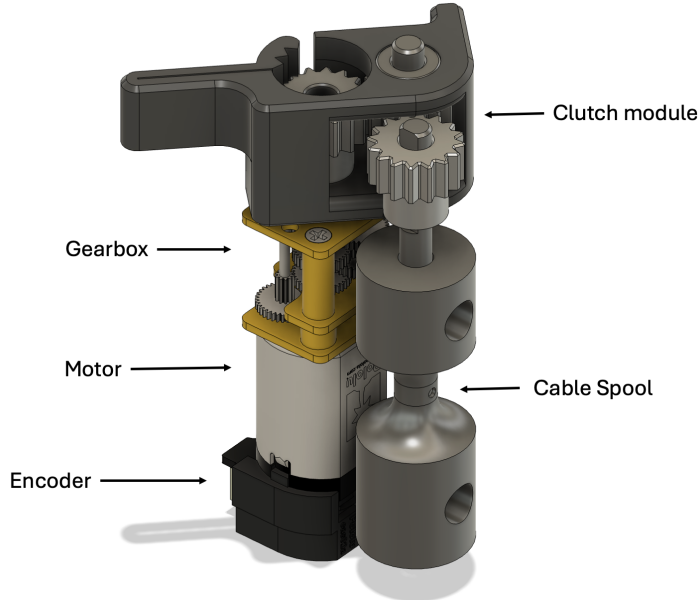


Figure 2.12: The internal components of the actuator. Note that screws, spacers, bearings, and the case have been omitted in this render to improve interpretability

### Compliant Ratchet

As noted by others in [24], the reliability of the JumpRoACH mechanism as originally described in [20] is low. Specifically, it can be difficult to engage and disengage the clutch, as the only force that the motor can exert on the clutch module is through friction between the motor shaft and the module. Given that the motor shaft is mounted to the clutch module via a bearing, this friction is minimal. This issue has been addressed with the use of one-way bearings [24], however one way bearings of the small size and low mass necessary for this actuator were not readily available.

Instead, a compliant ratchet mechanism was developed and used to augment the original JumpRoACH actuator. In this mechanism, when the motor rotates in the forward direction the teeth of the ratchet are free to move as the flexure can open (this can be seen in the middle image of figure 2.11). When the motor rotates backward the teeth cannot move out of the way of the gear's teeth as the flexure is pushed shut. This effectively locks the clutch module to the drive gear, ensuring that the motor torque is transmitted into the clutch module rather than the drivetrain, and allowing the clutch to be disengaged (this can be seen in the right image in figure 2.10). Additionally, the ratchet introduces a small amount of friction when operating in the forward direction, allowing the motor to apply to the clutch module the small torque necessary to re-engage the clutch.

### Actuator Construction

The actuator is primarily FFF 3D printed out of PLA. Experimentation showed that multi jet fusion (MJF) printed PA12 nylon, while significantly stronger, was too flexible and made tolerancing difficult. The remaining hardware is commercial off the shelf (CotS) parts such as bearings, shafts, and gears (bill of materials in appendix B.1).

Multiple motors were considered and tested to determine the most appropriate one. The motor selected is a Pololu 5228 with a 986:1 reduction gearbox on the

output. This motor was selected due to its high torque output of 10kgcm, built-in quadrature encoder, and low mass of 12g.

### 2.4.3 Actuator Performance

Several iterations of actuator were designed before it met the all the requirements outlined in section 2.4.2. The performance of the final actuator used on the robot is summarised in table 2.2.

Table 2.2: Performance of actuator used on robot

Specification	Theoretical Value	Observed Value
Mass (g)	40	40
Maximum Operating Current (A)	0.75	0.60
No-Load Winch Speed (mm/s)	5.5	5
Maximum Winching Force (N)	653*	60
Maximum Releasable Cable Tension (N)	245*	60
Clutch Disengagement Time (ms)	34	67
Cable Length Control Precision (mm)	±1.5mm	±1.5mm

\* Note that these values are extrapolated from motor performance measurements (current and torque) measurements at much lower loads (appendix C.1) and the testing of the motor showed failure at approximately 30% of these values



# Chapter 3

## Testing and Evaluation

### 3.1 Testing Methodology

#### 3.1.1 Data Collection

The performance of the robot was evaluated with respect to the objectives described in section 1.5. Experiments were performed with two methods of data collection: slow motion footage and 3D motion capture (OptiTrack Motion Capture System). The data collected was then post-processed to generate trajectories. With both methods of data collection, twelve nodes were tracked, each node being the end point of a strut.

The two methods of data collection have different sources of error (see section 3.3.6). Comparing the data generated by each method then allowed us to reduce uncertainty in the final results

#### 3.1.2 Data Analysis

##### Centre of Mass Estimation

The 12 nodes are all equidistant from the centroid (geometric centre) of the structure, and due to the symmetry of the six-bar icosahedron tensegrity structure, are arranged symmetrically about the centroid. Averaging the position of the tracked nodes then provides the centroid of the tensegrity structure. This is used as an estimate of the centre of mass (CoM).

##### Trajectory Estimation

When utilising slow motion footage, trajectories were extracted using purpose-designed software (Open Source Physics Tracker). A reference object of known length was placed next to the robot during filming to calibrate distance in each video. The software's built-in feature extraction tool was used to determine the position of each node relative to the reference object in every video frame. Node positions were manually entered for frames when feature extraction failed (e.g. when a node was partially occluded). Footage was recorded at a resolution of 1920x1080 and at a framerate of 240fps.

When utilising motion capture, each compliant node endcap was covered in retro-reflective tape to be visible to the infrared tracking camera. Motion tracking software (OptiTrack Motive) was then used to create a dataset containing the position of each node at each timestep. Data was recorded at 120fps. The positional data was then post processed to form a trajectory.

Useful measurements, primarily jump height and jump distance could then be extracted from the trajectory. Jump height is defined here as the greatest distance between the ground and the CoM of the robot during the jump, and jump distance is defined here as the horizontal difference between the CoM of the compressed robot pre-jump and the CoM when the robot first contacts the ground post-jump.

### Motion Capture Post-Processing

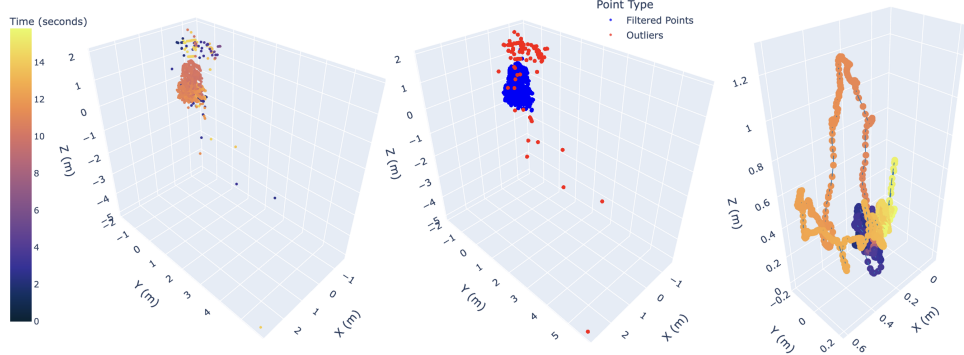


Figure 3.1: Example motion capture data processing pipeline. The raw data is collected (left), outliers are removed (middle), then individual datapoints are averaged and smoothed to generate a trajectory (right)

Infrared reflections from objects present in the motion capture space resulted in a noisy dataset, as the motion capture system registered other objects as additional nodes. Noise was also introduced by self occlusions, in which the robot would obscure one or several of its nodes from visibility to the cameras. Stray reflections are typically in irregular locations and so can be detected and removed. Local outlier factor anomaly detection (LOF) was used to remove these outliers (per scikit-learn implementation [25]) before the datapoints in each frame were averaged to produce the trajectory. The trajectory is then smoothed with a Savitzky-Golay filter [26] to address the noise introduced by occlusions (figure 3.1). The filter was implemented with SciPy [27].

## 3.2 Results

Test	Jump Height (m)	Jump Distance (m)	Take-Off Velocity (m/s)	Impact Efficiency (J/J)
High Jump 1	1.31	0.26	5.52	0.462
High Jump 2	1.24	0.34	5.28	0.422
Directional Jump 1	0.74	0.38	3.05	0.397
Directional Jump 2	0.73	0.38	3.07	0.402

Table 3.1: Jump test data. See section 2.1 for impact efficiency definition

### 3.2.1 Vertical Jumping

The robot demonstrated repeated vertical jumps of in excess of 2.0BL (1.22m) (table 3.2). An example of a vertical jump can be seen in figure 3.2. These jumps

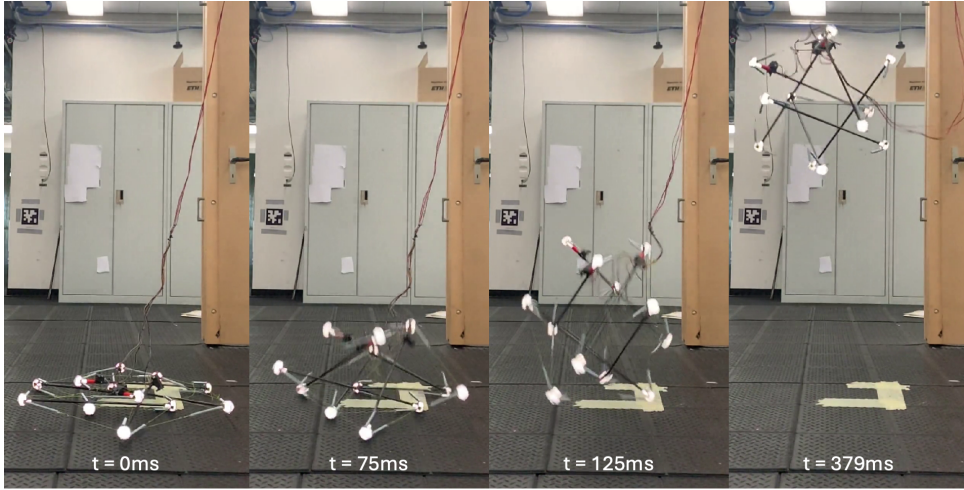


Figure 3.2: An example of a vertical jump from the “flat” configuration

were achieved by tensioning all three actuator cables equivalently, resulting in symmetric compression. Specifically, when the tension in all actuator cables reaches 50N (corresponding to a 45% reduction in actuator cable length), the structure collapses into a “flat” configuration (figure 3.3), which is the maximum amount that the tensegrity can be deformed along a single axis [17]. When the tension on the actuator cables is released, the resulting force as the structure transitions back to the rest form is orthogonal to the ground, inducing a vertical jump. This form of jump can be executed from two positions: all three actuated nodes on the ground or the mirror image of this reflected across the ground plane.

While the robot was able to achieve jumps of 1.3BL (0.79m) without any intervention, to achieve the “flat” configuration necessary for full height jumps a small external force would need to be applied. This was due to a self-intersection between nodes and struts that could cause the robot to get stuck during compression. This self-intersection could be addressed by manually ensuring the relevant nodes moved past the point at which they would get stuck during compression.

### 3.2.2 Directional Jumping

Directional jumping was demonstrated with heights of 1.2BL (0.73m) and distances of 0.6BL (0.37m) (table 3.2). An example of this can be seen in figure 3.5. For directional jumps, the three actuator cables are tensioned different amounts, which creates a resultant force on release that is not orthogonal to the ground. The greatest distances were achieved by decreasing the length of a single actuator cable by 40% and leaving the remaining actuator cables untensioned. The direction of the jump is along the axis of the tensioned actuator cable. One of three evenly spaced jump directions can then be chosen by selecting which actuator cable to tension (figure 3.4).

Smaller jumps of 0.2BL distance were achieved with the same process but by tensioning two, rather than one, actuator cables. Similar to the single actuator directional jump, this yields three discrete jump directions, however these directions are 60° offset from the three single actuator jump directions. This creates six total possible jump directions. However, with the two actuator directional jump, the distance travelled on landing was unpredictable and often larger than the distance travelled, making it impractical to use this jump technique (see section 3.2.5).

Directional jumping with more complex strategies was not successful. For varied

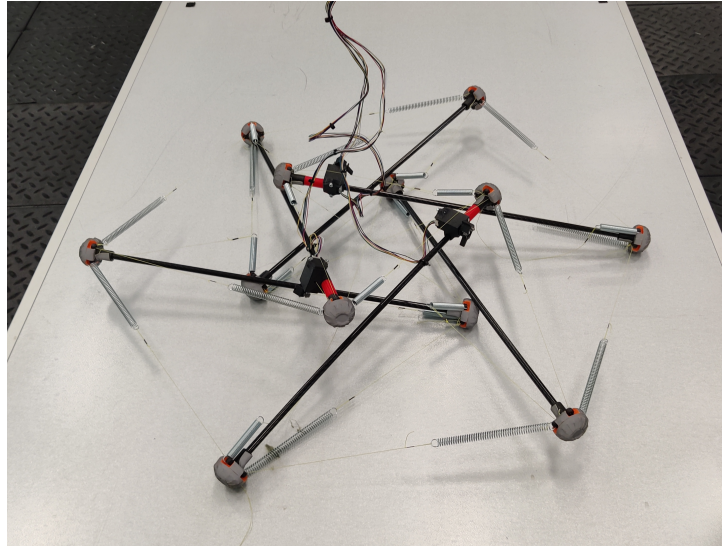


Figure 3.3: The “flat” configuration

tension on multiple actuator cables (which in theory would provide more precise control of jump direction), the direction of the jump was not well predictable. See section 3.3.3 for further discussion of this issue.

### 3.2.3 Self-Righting

Self-Righting was used as a method to achieve configuration-agnostic jumping. If the robot was not in the correct configuration for the desired jump, it was actuated to shift the CoM outside of the support polygon, tipping the robot onto an adjacent face (this is the punctuated rolling method described in section 1.3, and used by robots such as [7]). This could be repeated to roll across multiple faces until the robot was resting on the desired face. As vertical jumps and directional jumps have different initial configurations, different self-righting manoeuvres are required. While simulation suggested that self-righting would be possible from all configurations for both cases with the actuator topology described in section 2.4.1, unexpected real-world behaviour surrounding stable structural configurations (discussed in section 3.3.5) meant that self-righting was only possible from 11 of 20 faces.

### 3.2.4 Tensegrity Properties

#### Impact Resistance

The robot was successfully dropped from heights of up to 8.0BL (4.9m), resulting in ground impact velocities of 14.3BL/s (8.7m/s) without sustaining permanent damage. When dropped from 36.0BL (22.0m), the robot sustained damage to one actuator, limiting the ability to carry out vertical jumps and self-right. The tensegrity structure remained undamaged during all drop tests, even at a drop height of 36.0BL (22.0m).

#### Density and Change in Form

The robot’s bounding polyhedron is irregular (it has polygonal faces that are not congruent to each other) and non-convex (the are polygonal faces with internal

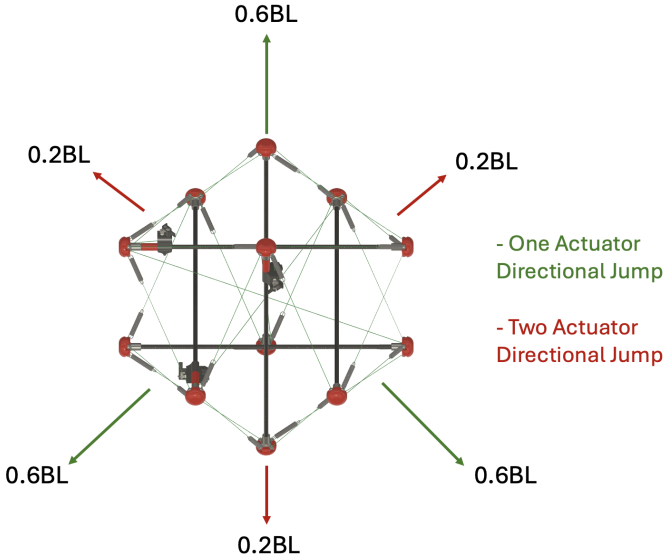


Figure 3.4: Jump directions demonstrated on hardware. In this top down view, the robot is positioned to jump in the direction of the upwards pointing arrow

angles between them that are larger than  $180^\circ$ ) in all configurations. Hence, we consider the volume of the tightest bounding ellipsoid to be a volume metric that is useful for comparing different configurations. At rest, this is a sphere with diameter of 0.61m, yielding a rest volume of  $0.119\text{m}^3$ . When flat (figure 3.3), the robot's bounding ellipsoid has a volume of  $0.0293\text{m}^3$ , meaning that by this metric a volume reduction in excess of 4x is possible without causing any damage. In addition, since the robot weighs 507g, in its rest configuration it has an extremely low density of  $4.26\text{kg/m}^3$ .

Several forms and compressions other than those useful for jumping were also tested to demonstrate the large variability in form (for example, figure 3.7). No damage was observed in any compressed configuration.

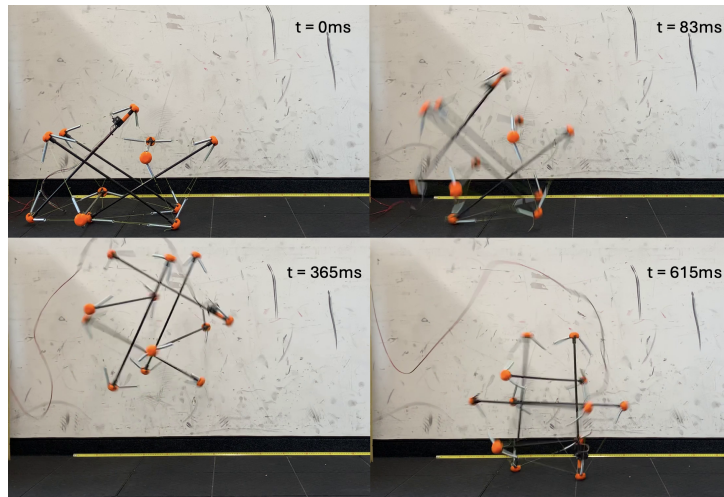


Figure 3.5: An example of a directional jump

### 3.2.5 Tumbling

The high overall compliance of the structure gives it a high coefficient of restitution, causing it to bounce on impact. Due to the complex geometry of the structure, this bouncing is accompanied by rotation around several axes. We describe this chaotic behaviour on impact as tumbling. In some cases, such as when utilising the single actuator directional jump described in section 3.2.2, the robot was imparted with angular momentum such that it would reliably tumble in the direction of the jump. This allowed it to cover greater distances before coming to a rest per jump (although all distances in this report are measured to the point of impact, not the point where the robot settles after tumbling). In general though, tumbling made it difficult to predict the final rest location of the robot, and in some cases the robot would even tumble back towards the start location.

### 3.2.6 Stability Bifurcation

The underlying tensegrity structure has a single stable configuration when at rest. We observed that, under certain intermediate compressions, there was a bifurcation that yielded two stable configurations of the structure. The energy required to transition between these two states is low, and the structure can transition between states under the influence of disturbances such as small differences in elastic cable pretensions, or the weight force of the robot itself. However, it was observed that the energy required to transition between these states increases as the structure is compressed further. The effect of this is that the final compressed configuration of the structure, being one of two stable states, is heavily dependent on disturbances that the system experiences during compression. We are not aware of this being noted anywhere else in the literature, perhaps because the actuation topology described in section 2.4.1 is novel.

## 3.3 Discussion

### 3.3.1 Impact Resistance

The robot was capable of surviving impacts well beyond the design objectives of 5.0BL drop height and 10.0BL/s impact velocity. This is likely due to several reasons, including:

1. Low density. The robot's low density of  $4.26\text{kg/m}^3$  means that it does not store a large amount of kinetic energy when in freefall and so there is less energy to dissipate.
2. High compliance. The high overall compliance of the robot means it can deform significantly on impact (figure 3.6). This allows it to dramatically extend the duration of the impact, which in turn reduces the impact force that it is subjected to.
3. Normal modes. The structure's complex geometry allows energy to be absorbed in several different modes of internal vibration. The energy can then be dissipated slowly through elastic losses in the structure.

### 3.3.2 Friction

It was observed that friction played a key role in jump performance. When the robot did not have good traction with the surface on which it was jumping, the jump height and jump distance (as defined in section 3.1.2) were reduced. Conversely,

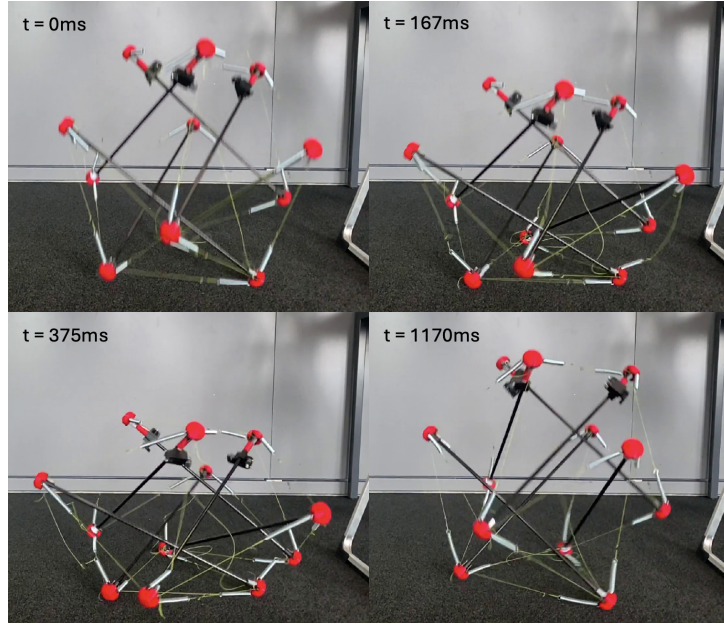


Figure 3.6: A drop test from 5.7BL (3.5m) with impact velocity 8.2BL/s (5.0m/s) showing how energy is absorbed by deformation of the structure. Note that the large amount of time (approximately 1.2s) that it takes the structure to deform and then return to its rest form results in a very long impact duration

when the node compliant endcaps were re-fabricated out of a higher friction TPU, jump height and jump distance increased. Analysis of the slow motion footage reveals that this is due to slippage of the nodes that are in contact with the ground - when friction is not high enough the feet slip against the ground, allowing the structure to distort more. The increased distortion results in more energy being lost to excitation of normal modes of the structure rather than being converted to translational motion.

### 3.3.3 Jumping

#### Losses

During directional jumps, which are necessary for locomotion, the robot was not able to cover distances as large as during vertical jumps. The arc length of the trajectory was 1.5m for directional jumps, compared to 2.6m for vertical jumps (although since a majority of the distance a vertical jump covers is in the vertical direction, it is less useful for locomotion). During the directional jumps, the robot had a lower impact efficiency (as defined in section 2.1) and a lower velocity at take off. There are several possible reasons, the most significant being that directional jumps were achieved using a single actuator, compared to the three actuators used for vertical jumps. This limits the amount of energy that can be stored in the structure. Additionally, the imbalance necessary to induce horizontal translation also causes a significant amount of rotation, meaning that more energy is converted to rotational motion that is not useful for translating. Finally, the structure is extremely good at absorbing energy in internal vibration of the structure (i.e. normal modes). While this is beneficial for impact resistance, it limits the amount of elastic potential that can be converted to translational kinetic energy. Further simulation may yield better jump techniques that reduce rotation, or better design parameters

that do not allow for as much excitation of normal modes.

### Efficacy of Jumping Locomotion

In order to be useful as a form of locomotion, the robot must be able to repeatedly jump in a controlled direction. Directional jumping was shown (section 3.2.2, however the precision of the directionality was limited. Specifically, the robot is limited to three discrete directions to jump useful distances. The exact cause for the poor performance seen on three-actuator directional jumps (described in 3.2.2) is not known, but may be because the system is sensitive to differences in pretension across the structure. Precisely setting pretension during construction of the structure was difficult, so pretensions vary by approximately 14% across the 24 structural cables.

Additionally, the issues seen with self-righting seen in section 3.2.3 mean that it may be possible to get stuck if the robot lands in a configuration from which it cannot self-right. Nevertheless, the results of testing are very promising, as they show that all of the individual components necessary for jumping locomotion are not just possible, but feasible.

#### 3.3.4 Form and Volume Control

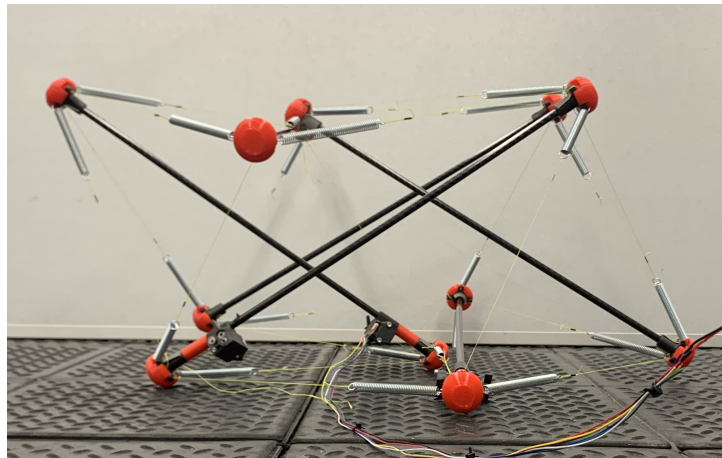


Figure 3.7: This partially compressed configuration has two large flat surfaces on the top and bottom, making the stacking of several robots in a confined space easier

The significant variability in form reinforces the robot's suitability for space exploration. The 4x reduction in volume that the robot exhibited is a key example of this, as room on spacecraft is typically very limited. In addition, various forms that make the robot more “packable”, such as those with large flat surfaces (figure 3.7) could also be useful for more efficient storage and transport.

While form changes due to actuation were the primary focus of this work, the robot’s ability to survive high impact energies suggest that it can sustain fairly large forces without damage. This means that potentially the robot could be compressed for transport significantly with high external forces, converting it to a more optimal configuration that it could not achieve with its own actuators.

### 3.3.5 Implementation Issues

There were several issues with the robot that were due to the implementation, and therefore unexpected as they were not predicted in simulation.

Firstly, the inability to self right from all possible configurations. In this case, the stability bifurcation described in section 3.2.6 was the main issue. In simulation, the mass force due to gravity was a large enough disturbance to bias the structure towards the correct state for self-righting. However, in the real structure, small differences in pretension in elastic cables was enough to overcome this force, and would bias the structure towards the incorrect state when in some configurations.

Secondly, there were structural self-intersections described in section 3.2.1. These were caused by the shape of the nodes (the structures that were used to mount cables and actuators to the end of struts). This could be resolved with minor changes to the design of the nodes, however it highlights how accurately predicting self-intersections is difficult when designing the robot in CAD. While the robot is thoroughly modelled in its rest state in CAD, the complex dynamics of the system make it difficult to model the motion the structure experiences during compression and jumping. Conversely, the simulator used to model the dynamics in [17] uses only an idealised model of the structure and cannot utilise the CAD model that describes the details of the implemented robot prototype.

### 3.3.6 Measurement Error

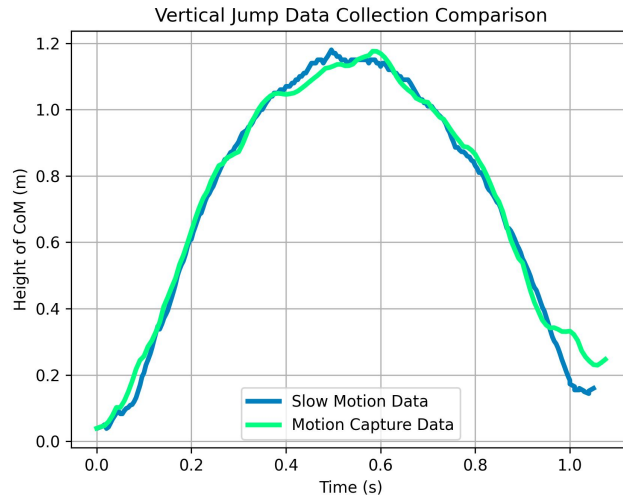


Figure 3.8: Comparison trajectories generated with data from slow motion footage and from motion capture. Both datasets are from the same vertical jump test.

Both data collection methods have sources of error that arise from their principle of operation. When filming slow motion footage, optical effects innate to video recording (specifically parallax and lens distortion) introduce error. Additionally, the trajectory is generated under the assumption that the robot does not move out of the plane of the recording (i.e. does not move towards or away from the camera). This assumption holds to varying degrees depending on the specific test.

When data is generated with motion capture, the motion capture system will occasionally lose sight of a node and be unable to track it for some number of frames. This is often due to self-occlusion as nodes pass behind struts and other

nodes during complex motion. This shifts the centroid estimation and causes it to have a constant offset error for the duration of the occlusion. As a result, noise is introduced to the trajectory. However, this noise is zero-mean, as at any given time each node has an equal probability of being occluded.

Quantifying the error introduced by the two different methods is difficult. However, both methods returned very similar trajectories (figure 3.8), with max jump height differing by <1% across tests. This indicates the error is minimal enough that it does not impact the results.

Regardless of the method used to collect data, the centroid is used as an estimate for the CoM. This is an accurate estimation for the underlying tensegrity structure, as it is symmetrical along three orthogonal axes. However, since the actuators are mounted off-centre, on the completed robot the centroid is not at precisely the same location as the CoM. The accuracy of the approximation varies as the structure changes form. At rest (i.e., uncompressed and static), this error is 52mm (8.5% BL), but can be as low as 12mm (2% BL) during full symmetric compression. Due to the difficulty associated with accurately tracking the CoM, this was deemed an acceptable level of error.

## 3.4 Evaluating Objectives

The objectives for the robot as defined in section 1.5 are considered in relation to the results of testing.

### High Jumping

The robot satisfies this objective as it can repeatably jump in excess of two body lengths. However, updates to the mechanical design to prevent the issues during compression described section 3.2.1 would allow the robot to achieve this with less human intervention. Even without these applications of external forces the robot still satisfies the requirement as it can still jump 1.3BL.

### Directional Jumping

The robot partially satisfies this objective. Direct control over the direction in which the robot jumps is possible, but only three discrete directions are possible for jumping useful distances. In lower gravity other directions may be possible since smaller forces that did not induce a jump in earth gravity may do so in lower gravity. Alternatively, a different actuation topology may improve this.

### Favourable Tensegrity Properties

All the desired tensegrity properties (resistance to impact damage, ability to change form significantly, and high strength to mass ratio) were demonstrated. Resistance to impact damage significantly exceeded expectations.

### Configuration Agnostic Jumping

This objective was partially achieved, in that self righting was shown to be possible on the structure selected with the actuator topology designed. However, real world limitations prevented self-righting from all possible faces

### Use of Tensegrity Structure

This objective was satisfied. All the desired properties that were demonstrated were done so by actuating the underlying structure.

### 3.5 Comparison to Existing Work

A comparison to other similar tensegrity robots (table 3.2) is provided to contextualise this report and make clear the gap in the literature that this robot fills. Most existing robots are not capable of jumping [3]. Those that are capable of jumping typically cannot exceed 1.0BL in height during jumps (for example [14] [13]). Some works can only jump vertically [15]. Additionally, most jumping tensegrity robots do not jump by deforming the underlying tensegrity structure, and instead require additional actuators (for example [13] [12]). A robot that addresses most of these issues is proposed in [15], but most capability was demonstrated only in simulation and not on hardware.

Table 3.2: Comparison with existing similar tensegrity robots

	SUPERball v2 [7]	Spikebot [13]	SMA Spring Jumper [14]	Soft Planetary Lander [15]	Flying Random Explorer [12]	This Work
Capable of Jumping >0.1BL	No	Yes	Yes	Yes	Yes	Yes
Capable of Jumping >1.0BL	No	No	No	Yes	Yes	Yes
Capable of Directional Jumping	No	Yes	Yes	No*	No**	Yes
Jumping without additional actuators	Yes	No	Yes	Yes	No	Yes
Demonstrated on Hardware	Yes	Yes	Yes	No	Yes	Yes

\* Individual robots were not capable of directional jumping, however several robots could be combined in a lattice to provide directionality

\*\* The robot's jump trajectories were random, so while it could occasionally jump in a direction it was not controllable



# Chapter 4

## Conclusion

### 4.1 Summary of Findings

This work presents the development and testing of a novel tensegrity robot designed to jump utilising the underlying tensegrity structure. The key objectives of high jumping, demonstrating favourable tensegrity properties, and jumping by actuating the underlying tensegrity structure were fully satisfied. Additionally, the objectives of directional jumping and configuration-agnostic jumping were partially satisfied.

This demonstrates the feasibility of the jumping by actuating the tensegrity structure as a form of locomotion for tensegrity robotics. There are some issues that the robot was not capable of addressing, namely limited choices for jump direction and problems surrounding structural self-intersections. However these can be addressed with minor updates to the robot design in future works. Additionally, the robot was capable of surviving impacts at velocities well above expectations. Ultimately, the robot described in this work is a first prototype developed to show feasibility of a novel concept, and in that sense it has been successful.

### 4.2 Limitations

#### Hardware

The issues in the implementation of the robot described in section 3.3.5 prevented the robot from fully demonstrating all the desired behaviour. Updating minor aspects of the robot’s design, such as adjusting the shape of the nodes to prevent them from getting stuck during certain compressions, could address this. However, there are more significant limitations with the design itself. For one, the robot is tethered and must be powered and controlled externally. This limitation is insignificant in the context of demonstrating feasibility, but is a more serious issue if the robot is further developed for mobile and/or autonomous operation.

#### Performance

While this work demonstrates a robot that is a measurable improvement on existing jumping tensegrities, it is still significantly outperformed by other forms of locomotion in many contexts. For example, wheeled rovers are likely to be faster and more stable on many terrains. Additional work is required to broaden the scope in which jumping tensegrity robots are competitive with more conventional mobile robots.

### Simulation

The work done in simulation to determine appropriate prototype parameters and develop jump strategies was essential. However, as noted in section 3.3.5, the simulation tools (in particular the Nasa Tensegrity Robotics Toolkit used in [17]) still make significant simplifying assumptions about the robot's design and physical structure. This made it difficult to validate certain decisions when designing the prototype, and resulted in effects such as those observed in 3.2.6.

## 4.3 Further Research

### Highly Dynamic Reversible Actuators

Currently, actuation is fairly slow, with jumps such as full-compression vertical jumps taking as much as a minute for the actuators to fully compress the structure. Additionally, the actuators can increase tension with high precision but only have binary control over the release of tension and cannot decrease tension by small increments. New actuators that address these shortfalls would expand the scope of research greatly, by allowing the development of more complex gaits and mid-air actuation of the structure. Mid-air actuation in particular could be a good method to counter the tumbling described in section 3.2.5 by controlling the impact conditions.

### Closed Loop Control

Closed loop control of the structure is another avenue with significant potential. In this work, control strategies were generated in simulation then implemented on the robot manually. Feedback control could yield significantly better performance. Additionally, given the complex dynamics of the structure, reinforcement learning could yield better policies than the current approach of manually developing candidate policies then evaluating them in simulation.

### Varied Terrain

This work only explores locomotion in a controlled and level laboratory environment. Given the complexity associated with terrain in the real world, exploring the performance of both the robot and of jumping as a form of locomotion in more complex environments could yield useful insight into applicability in real-world contexts.

### Expanded Locomotion Capability

Finally, while jumping has several advantages over other locomotion strategies, implementing more conventional tensegrity locomotion strategies (such as punctuated rolling or shuffling) in conjunction with jumping could significantly increase utility. A robot that could both jump and roll could, for example, utilise jumping when needing to cover large distances and switch to rolling when it is necessary to cover a small area with more precision.

# Bibliography

- [1] R. Motro, *Tensegrity: structural systems for the future*. Elsevier, 2003.
- [2] R. Skelton, R. Adhikari, J.-P. Pinaud, W. Chan, and J. Helton, “An introduction to the mechanics of tensegrity structures,” in *Proceedings of the 40th IEEE Conference on Decision and Control (Cat. No.01CH37228)*, vol. 5, 2001, pp. 4254–4259 vol.5.
- [3] D. S. Shah, J. W. Booth, R. L. Baines, K. Wang, M. Vespignani, K. Bekris, and R. Kramer-Bottiglio, “Tensegrity robotics,” *Soft Robotics*, vol. 9, no. 4, pp. 639–656, 2022, pMID: 34705572.
- [4] B. Trimmer, “An interview with nasa principal investigator vytas sunspiral: expert opinion on the advantages and limitations of soft robotics,” *Soft Robotics*, vol. 2, no. 2, pp. 51–58, 2015.
- [5] Y. Liu, Q. Bi, X. Yue, J. Wu, B. Yang, and Y. Li, “A review on tensegrity structures-based robots,” *Mechanism and Machine Theory*, vol. 168, p. 104571, 2022.
- [6] S. Lessard, D. Castro, W. Asper, S. D. Chopra, L. B. Baltaxe-Admony, M. Teodorescu, V. SunSpiral, and A. Agogino, “A bio-inspired tensegrity manipulator with multi-dof, structurally compliant joints,” in *2016 IEEE/RSJ International Conference on Intelligent Robots and Systems (IROS)*, 2016, pp. 5515–5520.
- [7] M. Vespignani, J. M. Friesen, V. SunSpiral, and J. Bruce, “Design of superball v2, a compliant tensegrity robot for absorbing large impacts,” in *2018 IEEE/RSJ International Conference on Intelligent Robots and Systems (IROS)*, 2018, pp. 2865–2871.
- [8] C. Paul, F. Valero-Cuevas, and H. Lipson, “Design and control of tensegrity robots for locomotion,” *IEEE Transactions on Robotics*, vol. 22, no. 5, pp. 944–957, 2006.
- [9] M. Zhang, X. Geng, J. Bruce, K. Caluwaerts, M. Vespignani, V. SunSpiral, P. Abbeel, and S. Levine, “Deep reinforcement learning for tensegrity robot locomotion,” in *2017 IEEE International Conference on Robotics and Automation (ICRA)*, 2017, pp. 634–641.
- [10] K. Kim, L.-H. Chen, B. Cera, M. Daly, E. Zhu, J. Despois, A. K. Agogino, V. SunSpiral, and A. M. Agogino, “Hopping and rolling locomotion with spherical tensegrity robots,” in *2016 IEEE/RSJ International Conference on Intelligent Robots and Systems (IROS)*, 2016, pp. 4369–4376.
- [11] S. Savin, A. Al Badr, D. Devitt, R. Fedorenko, and A. Klimchik, “Mixed-integer-based path and morphing planning for a tensegrity drone,” *Applied Sciences*, vol. 12, p. 5588, 05 2022.

- [12] S. Mintchev, D. Zappetti, J. Willemin, and D. Floreano, “A soft robot for random exploration of terrestrial environments,” in *2018 IEEE International Conference on Robotics and Automation (ICRA)*. IEEE, 2018, pp. 7492–7497.
- [13] J. Jeong, I. Kim, Y. Choi, S. Lim, S. Kim, H. Kang, D. Shah, R. Baines, J. W. Booth, R. Kramer-Bottiglio, and S. Y. Kim, “Spikebot: A multigait tensegrity robot with linearly extending struts,” *Soft Robotics*, vol. 11, no. 2, pp. 207–217, 2024, pMID: 37819709.
- [14] Y. S. Chung, J.-H. Lee, J. H. Jang, H. R. Choi, and H. Rodrigue, “Jumping tensegrity robot based on torsionally prestrained sma springs,” *ACS Applied Materials & Interfaces*, vol. 11, no. 43, pp. 40793–40799, 2019, pMID: 31512858.
- [15] K. Garanger, I. del Valle, M. Rath, M. Krajewski, U. Raheja, M. Pavone, and J. J. Rimoli, *Soft Tensegrity Systems for Planetary Landing and Exploration*, pp. 841–854.
- [16] V. SunSpiral, G. Gorospe, J. Bruce, A. Iscen, G. Korbel, S. Milam, A. K. Agogino, and D. Atkinson, “Tensegrity based probes for planetary exploration : Entry , descent and landing ( edl ) and surface mobility analysis,” 2013.
- [17] D. Bozinovski, “Simulation of high jumping tensegrity robot for adaptable space locomotion,” *ETH Zurich Research Collection*, 2024.
- [18] M. Vespiagnani, C. Ercolani, J. M. Friesen, and J. Bruce, “Steerable locomotion controller for six-strut icosahedral tensegrity robots,” in *2018 IEEE/RSJ International Conference on Intelligent Robots and Systems (IROS)*, 2018, pp. 2886–2892.
- [19] “Overview of materials for Epoxy/Carbon Fiber Composite — matweb.com,” [https://www.matweb.com/search/datasheet\\_print.aspx?matguid=39e40851fc164b6c9bda29d798bf3726](https://www.matweb.com/search/datasheet_print.aspx?matguid=39e40851fc164b6c9bda29d798bf3726), [Accessed 22-06-2024].
- [20] G.-P. Jung, C. S. Casarez, J. Lee, S.-M. Baek, S.-J. Yim, S.-H. Chae, R. S. Fearing, and K.-J. Cho, “Jumproach: A trajectory-adjustable integrated jumping-crawling robot,” *IEEE/ASME Transactions on Mechatronics*, vol. 24, no. 3, pp. 947–958, 2019.
- [21] J. Hwangbo, V. Tsounis, H. Kolvenbach, and M. Hutter, “Cable-driven actuation for highly dynamic robotic systems,” in *2018 IEEE/RSJ international conference on intelligent robots and systems (IROS)*. IEEE, 2018, pp. 8543–8550.
- [22] J.-B. Izard, M. Gouttefarde, M. Michelin, O. Tempier, and C. Baradat, “A reconfigurable robot for cable-driven parallel robotic research and industrial scenario proofing,” in *Cable-driven parallel robots*. Springer, 2012, pp. 135–148.
- [23] J. Friesen, A. Pogue, T. Bewley, M. de Oliveira, R. Skelton, and V. Sunspiral, “Ductt: A tensegrity robot for exploring duct systems,” in *2014 IEEE International Conference on Robotics and Automation (ICRA)*, 2014, pp. 4222–4228.
- [24] Y. Ma, Y. Wei, and D. Kong, “A biologically inspired height-adjustable jumping robot,” *Applied Sciences*, vol. 11, no. 11, 2021.

- [25] F. Pedregosa, G. Varoquaux, A. Gramfort, V. Michel, B. Thirion, O. Grisel, M. Blondel, P. Prettenhofer, R. Weiss, V. Dubourg, J. Vanderplas, A. Passos, D. Cournapeau, M. Brucher, M. Perrot, and E. Duchesnay, “Scikit-learn: Machine learning in Python,” *Journal of Machine Learning Research*, vol. 12, pp. 2825–2830, 2011.
- [26] A. Savitzky and M. J. E. Golay, “Smoothing and differentiation of data by simplified least squares procedures.” *Analytical Chemistry*, vol. 36, no. 8, pp. 1627–1639, 1964.
- [27] P. Virtanen, R. Gommers, T. E. Oliphant, M. Haberland, T. Reddy, D. Cournapeau, E. Burovski, P. Peterson, W. Weckesser, J. Bright, S. J. van der Walt, M. Brett, J. Wilson, K. J. Millman, N. Mayorov, A. R. J. Nelson, E. Jones, R. Kern, E. Larson, C. J. Carey, İ. Polat, Y. Feng, E. W. Moore, J. VanderPlas, D. Laxalde, J. Perktold, R. Cimrman, I. Henriksen, E. A. Quintero, C. R. Harris, A. M. Archibald, A. H. Ribeiro, F. Pedregosa, P. van Mulbregt, and SciPy 1.0 Contributors, “SciPy 1.0: Fundamental Algorithms for Scientific Computing in Python,” *Nature Methods*, vol. 17, pp. 261–272, 2020.
- [28] R. G. Budynas, J. K. Nisbett *et al.*, *Shigley’s mechanical engineering design*. McGraw-Hill New York, 2011, vol. 9.
- [29] StructX, “Hollow Circle (Annulus) - Geometric Properties — structx.com,” [https://structx.com/Shape\\_Formulas\\_014.html](https://structx.com/Shape_Formulas_014.html), [Accessed 23-06-2024].
- [30] usdp, “Spring Rate - WB Jones — springsfast.com,” <https://www.springsfast.com/resources/blog/spring-rate/#:~:text=The%20spring%20rate%20is%20a,are%20always%20happy%20to%20help!>, [Accessed 23-06-2024].



# Appendix A

# Additional Material

## A.1 Feasibility Modelling

While the six-bar icosahedron tensile-structure has 24 elastic cables, in some compressed configurations (such as the “flat” configuration seen in figure 3.3) as few as 6 elastic elements may actually be tensioned. Hence, we conservatively assume that for a jump, only 6 elastic elements are storing energy. Next, we simplify the geometry and assume that each elastic element experiences the maximum actuator force. In reality, this is only sometimes true and is dependant on the way in which the structure is compressed. Since the extension force  $F_E$  for each elastic element with stiffness  $k$  follows Hooke’s law of  $F_E = kx$  for an extension of length  $x$  and elastic potential energy  $E_{EP}$  stored in the elastic element follows  $E_E = \frac{1}{2}kx^2$ , it follows that for a maximum actuator force  $F_{max}$  the elastic potential energy is

$$E_{EP} = \frac{F_{max}^2}{2k} \quad (\text{A.1})$$

We include an impact efficiency factor  $e_i$  that describes what proportion of this potential energy is converted into translational kinetic energy in the vertical direction  $E_{KV}$  (note that some of this potential energy may be converted to kinetic energy that is not directly useful, such as rotation or internal normal modes of the structure), and consider the fact that there are 6 extended elastic elements. This yields

$$E_{KV} = \frac{3e_i F_{max}^2}{k}$$

At height  $h$  during a jump, with robot mass  $m$  and in gravity  $g$ , the gravitational potential energy is

$$E_{GP} = mgh$$

Assuming no losses to air resistance (these losses would likely be low given small surface area and low velocity of the tensegrity structure), at the highest point of the jump the kinetic energy has been entirely converted to gravitational potential, so  $E_{KV} = E_{GP}$ . Solving for the maximum height  $h_{max}$  gives

$$h_{max} = \frac{3e_i F_{max}^2}{km} \quad (\text{A.2})$$

The maximum actuator force is fixed at 50N, and the mass is set at 600g (this is derived by assuming a symmetric mass distribution of 100g per strut and massless cables). Equation A.2 is then plotted in figure 2.1 for varying values of spring stiffness and impact efficiency.

## A.2 Scaling Laws

Consider strut length as a measure of robot size. Indeed, the diameter (tightest bounding sphere) of the robot is proportional to strut length. For a robot whose size is within a single order of magnitude, it is assumed that the mass of hardware other than struts is constant regardless of strut length; for example the same node part which attaches cables to the end of the strut can be used whether the strut is 200mm or 300mm long. For a given strut diameter, the mass of the robot then scales linearly with strut length, so  $m \propto l$ . Given that energy stored per spring is described by equation A.1 (note that this is independent of size, the energy to mass ratio follows

$$\frac{E_{EP}}{m} \propto \frac{F_{max}^2}{kl} \quad (\text{A.3})$$

## A.3 Strut Failure

### A.3.1 Average Impact Force

To determine the load that each strut must sustain, an upper limit on the compressive force a strut may experience was estimated. The worst case is considered, where the entire force of an impact is imparted on a single strut, and the strut is orthogonal to the ground. This is not possible on a flat surface and when the structure is in its equilibrium position due to the geometry of the structure, but may occur if the surface is not flat or the structure is vibrating internally. The maximum impact energy  $E_{impact}$  can be determined, by conservation of energy, from the gravitational potential energy. Hence,

$$E_{impact} = mgh$$

Assuming that the robot is at rest when dropped. The velocity of the robot at impact  $v_{impact}$  then follows

$$v_{impact} = (2gh)^{\frac{1}{2}}$$

The impulse of this impact is given by

$$Impulse = m\Delta v = F_{impact,avg}t_{impact}$$

where  $F_{impact,avg}$  is the average force during impact,  $t_{impact}$  is the duration of the impact, and  $\Delta v$  is the change in velocity during impact. Assuming the structure absorbs all the energy of the drop,  $\Delta v = v_{impact}$ . Then,

$$F_{impact,avg} = \frac{m(2gh)^{\frac{1}{2}}}{t_{impact}} \quad (\text{A.4})$$

### A.3.2 Failure Modes

Given that the strut experiences only compressive forces in a 0-class tensegrity structure [2], only two failure modes need to be considered: compressive yielding and buckling. Compressive yield load  $F_{yield}$  is given by

$$F_{yield} = \sigma_{yield}A_{strut} \quad (\text{A.5})$$

Where  $\sigma_{yield}$  is the compressive yield strength of the material and  $A_{strut}$  is the cross-sectional area of the strut, in this case given by

$$A_{strut} = \pi(r_{outer}^2 - r_{inner}^2)$$

where  $r_{outer}$  and  $r_{inner}$  are the outer and inner diameters of the tube.

The buckling load  $F_{buckle}$  can be computed using Euler's critical load [28], given by

$$F_{buckle} = \frac{\pi^2 EI}{(Kl)^2} \quad (\text{A.6})$$

Where  $E$  is the modulus of elasticity of the material,  $I$  is the second moment of area of the cross section of the strut,  $K$  is the effective length factor, and  $l$  is the length of the strut.

The values in table A.1 are used to generate figure 2.5 and compute the values described in section 2.3.4:

Table A.1: Strut Physical Properties

Property	Value
Modulus of Elasticity ( $E$ )	101GPa [19]
Second Moment of Area ( $I$ )	$\frac{\pi}{2}(r_{outer}^4 - r_{inner}^4) \text{ m}^4$ [29]
Effective Length Factor ( $K$ )	1.0*
Strut Length ( $l$ )	500mm
Compressive Yield Strength ( $\sigma_{yield}$ )	758MPa [19]

\* Since the strut is unconstrained at both ends

## A.4 Spring Modelling

### Mass

The spring is modelled as a set of  $n$  stacked tori. Since each torus with wire diameter  $d_{wire}$  and coil diameter  $D_{spring}$  has volume  $v_{torus} = \pi^2 D_{spring}(\frac{d_{wire}}{2})^2$ , the mass of the spring can be expressed as

$$m_{spring} = \frac{n\rho_{wire}\pi^2 d_{wire}^2 D_{spring}}{4} \quad (\text{A.7})$$

Where  $\rho_{wire}$  is the density of the spring wire. Additionally, the spring rate  $k$  for a spring with modulus of rigidity  $G$  can be expressed as [30]

$$k = \frac{Gd_{wire}^4}{8D_{spring}^3 n} \quad (\text{A.8})$$

Combining these yields

$$m_{spring} = \alpha d_{wire}^{\frac{8}{3}} l_{spring}^{\frac{2}{3}} \quad (\text{A.9})$$

Where  $l_{spring} = nd_{wire}$  is the length of the spring and  $\alpha = \frac{1}{8}\pi^2\rho_{wire}(\frac{G}{k})^{1/3}$  is a constant determined by the properties of spring material and the desired spring rate.

### Maximum Force

To compute the maximum force that a spring may experience during a collision, the model and worst case assumptions from section A.3 were used. Under these assumption, only a single node is impacting the ground, meaning that only four of the 24 elastic elements are engaged. Assuming equal distribution of force across these four, the dynamic load on each spring is

$$F_{max} = \left( \frac{1}{2} kmgh_{max} \right)^{\frac{1}{2}}$$

This was used when selecting appropriate springs for the robot, and can be seen in figure A.1

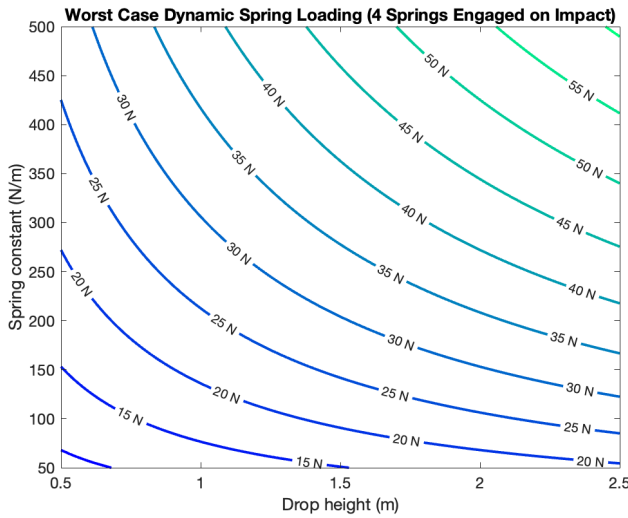


Figure A.1: Dynamic loading on springs for worst-case impact configuration

## Appendix B

# Bills of Materials

### B.1 Actuator Bill of Materials

Part Name	Part Details	Quantity
Motor	Pololu 5228	1
Case	3D printed PLA	1
Lid	3D printed PLA	1
Pulley	3D printed PLA	1
Clutch Module	3D printed PLA	1
Pulley Shaft	$\varnothing$ 3mmx50mm steel shaft	1
Gear Shaft	$\varnothing$ 3mmx15mm steel shaft	1
Space	Nylon M3x3mm washer	1
Cable	$\varnothing$ 0.29mm braided eight-strand UHMWPE	1
Case Screw	M3x8mm socket head screw	2
Motor Mount Screw	M1.6x5mm flat head machine screw	2
Gear	RS Pro 1827882 16t Spur Gear, 0.5mod	3
Bearing	Misumi B673ZZ ball bearing	4

### B.2 Series Elastic Cable Bill of Materials

Part Name	Part Details	Quantity
Cable	$\varnothing$ 0.29mm braided eight-strand UHMWPE	1
Crimp	$\varnothing$ 1.0mmx5mm copper fishing line crimp	1
Spring	Sodemann Industrial 505 spring, 410N/m	1

### B.3 Node Bill of Materials

Part Name	Part Details	Quantity
Node Body	3D Printed PLA	1
Node Compliant Endcap	3D Printed TPU	1
Screw Insert	Brass M3x5mm heat-press insert	2
Washer	M3x0.5mm steel washer	2
Cable Mounting Screw	M3x4mm button head hex screw	2

### B.4 Robot Bill of Materials

Part Name	Part Details	Quantity
Strut	$\varnothing 8\text{mm} \times 500\text{mm}$ CFRP tube, 0.5mm wall thickness	6
Node	See appendix B.3	6
Decoupling Bumper	3D Printed TPU	3
Actuator	See appendix B.1	3
Structural Cable	See appendix B.2	24

## Appendix C

### Datasheets

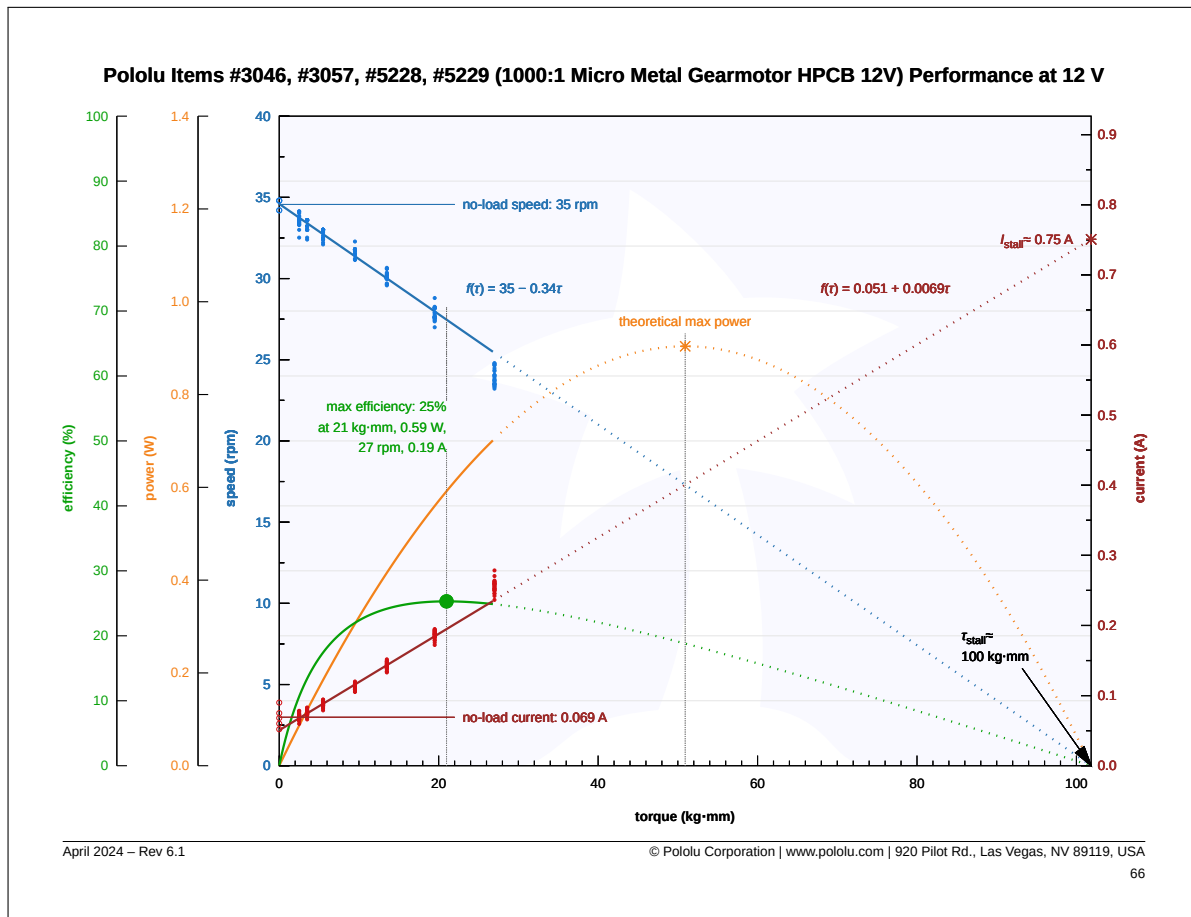


Figure C.1: Datasheet for motor used in actuator